Stochastic Parameterization and El Niño–Southern Oscillation

H. M. CHRISTENSEN

Atmospheric, Oceanic and Planetary Physics, University of Oxford, Oxford, United Kingdom

JUDITH BERNER AND DANIELLE R. B. COLEMAN

National Center for Atmospheric Research, Boulder, Colorado

T. N. PALMER

Atmospheric, Oceanic and Planetary Physics, University of Oxford, Oxford, United Kingdom

(Manuscript received 8 February 2016, in final form 18 August 2016)

ABSTRACT

El Niño–Southern Oscillation (ENSO) is the dominant mode of interannual variability in the tropical Pacific. However, the models in the ensemble from phase 5 of the Coupled Model Intercomparison Project (CMIP5) have large deficiencies in ENSO amplitude, spatial structure, and temporal variability. The use of stochastic parameterizations as a technique to address these pervasive errors is considered. The multiplicative stochastically perturbed parameterization tendencies (SPPT) scheme is included in coupled integrations of the National Center for Atmospheric Research (NCAR) Community Atmosphere Model, version 4 (CAM4). The SPPT scheme results in a significant improvement to the representation of ENSO in CAM4, improving the power spectrum and reducing the magnitude of ENSO toward that observed. To understand the observed impact, additive and multiplicative noise in a simple delayed oscillator (DO) model of ENSO is considered. Additive noise results in an increase in ENSO amplitude, but multiplicative noise can reduce the magnitude of ENSO, as was observed for SPPT in CAM4. In light of these results, two complementary mechanisms are proposed by which the improvement occurs in CAM. Comparison of the coupled runs with a set of atmosphere-only runs indicates that SPPT first improve the variability in the zonal winds through perturbing the convective heating tendencies, which improves the variability of ENSO. In addition, SPPT improve the distribution of westerly wind bursts (WWBs), important for initiation of El Niño events, by increasing the stochastic component of WWB and reducing the overly strong dependency on SST compared to the control integration.

1. Introduction

El Niño–Southern Oscillation (ENSO) is the dominant mode of tropical variability on interannual time scales (Neelin et al. 1998). It describes a set of coupled ocean–atmosphere phenomena describing an irregular cycle of warming and cooling in the eastern tropical Pacific associated with a collocated variation in sea level pressure (Rasmusson and Carpenter 1982). Through atmospheric teleconnections, an ENSO warm or cold event impacts weather across the globe. While the impact is strongest in regions adjacent to the tropical Pacific—for example, with the warm phase associated with heavy rain in Peru and drought in Indonesia (Sarachik and Cane 2010)—ENSO also impacts the global tropics, affecting the intensity of precipitation in the Indian monsoon (Ropelewski and Halpert 1996) and the number of hurricanes hitting North America (Bove et al. 1998). In fact, ENSO's effects are sufficiently far reaching as to impact extratropical latitudes, including the likelihood of drought in the North American midwest (Ropelewski and Halpert 1987), although the response to a particular warm or cold event is less predictable. Because of these numerous teleconnections, ENSO is a significant source of skill in

Denotes Open Access content.

Corresponding author address: Hannah M. Christensen, Clarendon Laboratory, Atmospheric, Oceanic and Planetary Physics, Parks Road, Oxford OX1 3PU, United Kingdom.
E-mail: h.m.christensen@atm.ox.ac.uk

DOI: 10.1175/JCLI-D-16-0122.1

seasonal forecasts (Barnett and Preisendorfer 1987), so it is important that global circulation models (GCMs) can capture and predict this mode of variability.

There are two main hypotheses proposed to explain ENSO (Neelin et al. 1998). The first is the delayed oscillator (DO) model, where for a strong enough coupling between atmosphere and ocean, the system is unstable and exhibits regular oscillations (Suarez and Schopf 1988). The second hypothesis is the stochastic excitation model: for a stable system that exhibits nonnormality, small disturbances can initially grow before ultimately decaying. Exciting such a system with stochastic perturbations leads to irregular oscillations similar to ENSO (McWilliams and Gent 1978; Penland and Sardeshmukh 1995). Analysis of observations indicates that the ''real'' ENSO is not necessarily in the unstable regime but could be a stable system driven by noise (Penland 1996; Chang et al. 1996). Other studies suggest a self-maintaining ENSO (Jin et al. 1996; Grieger and Latif 1994). It is possible that the observed ENSO results from a combination of these two kinds of mechanisms. A third mechanism is that ENSO could be a nonlinear self-sustaining oscillation, although this hypothesis seems less likely (Jin et al. 1996).

Whether the system is linearly stable or unstable, many papers support the importance of stochastic processes in forcing ENSO (Penland and Sardeshmukh 1995). There is evidence that decadal variability in ENSO amplitude, along with its associated predictability, is a result of stochastic forcing from the atmosphere (Flügel et al. 2004; Yeh and Kirtman 2006), where the sensitivity of ENSO predictability to this stochastic forcing is a function of time of year and the atmospheric variable forced (Kleeman and Moore 1997; Moore and Kleeman 1999), as well as the frequency characteristics of the stochastic forcing (Roulston and Neelin 2000). In general, the importance of atmospheric stochastic perturbations is recognized in ocean modeling, where there has been a long history of representing the influence of the atmosphere on the ocean using a stochastic process (Hasselmann 1976).

Despite the evidence of the importance of stochastic forcing in the modeling and prediction of ENSO, the climate modeling community has largely focused on deterministic representation of the components of the coupled ocean–atmosphere system that are important for ENSO. In recent years there has been much improvement in the representation of ENSO in coupled GCMs (Flato et al. 2013; Guilyardi et al. 2009). This is due in part to increased resolution but also due to improvements in the physical parameterization schemes (Neale et al. 2008). However, models still exhibit large systematic errors in both mean climate and simulated variability (Guilyardi et al. 2009). Several studies indicate that errors in coupled GCMs can be attributed to deficiencies in the atmospheric model (Braconnot et al. 2007; Sun et al. 2009), but despite this progress, the models in phase 5 of the Coupled Model Intercomparison Project (CMIP5) show large deficiencies in ENSO amplitude, spatial structure, and temporal variability, and improvement in the CMIP5 ensemble compared to CMIP3 can largely be attributed to fewer poor-performing models (Flato et al. 2013).

A new but rapidly growing area of research in atmospheric modeling involves representing atmospheric processes as a combination of a predictable deterministic component and an unpredictable stochastic component. While traditional deterministic parameterization schemes can represent the bulk average effect of unresolved subgrid-scale processes on the resolved flow, stochastic parameterization schemes have been developed to represent the variability of unresolved processes (i.e., the stochastic component of the atmospheric flow; Palmer et al. 2009). Such schemes have been shown to have a beneficial effect on the spread and mean state for medium-range and seasonal forecasts (Buizza et al. 1999; Palmer et al. 2009; Weisheimer et al. 2014). Seasonal forecasts show evidence for reduced forecast biases and improvements in intraseasonal variability such as the Madden–Julian oscillation (MJO; Berner et al. 2012; Weisheimer et al. 2014).

There is also increasing evidence that stochastic parameterization of unresolved processes could be beneficial for the climate of an atmospheric model. Including a zero-mean noise term into a GCM can cause a shift in the mean climate resulting from nonlinearities in the system (Sardeshmukh et al. 2001, 2003; Williams 2012); this can reduce model biases, improving the mean climate (Berner et al. 2008). Even in the absence of nonlinearities, a ''noise-induced drift'' can occur in the presence of multiplicative noise but not additive white noise (e.g., Berner et al. 2016, their Fig. 1). A second mechanism through which stochastic schemes can improve the modeled climate is by improving the climate variability (Lin and Neelin 2000, 2003), which can occur through enabling the climate simulator to explore other flow regimes (Christensen et al. 2015; Dawson and Palmer 2015); such ''noise-induced transitions'' can occur in the presence of either additive or multiplicative noise (e.g., Berner et al. 2016, their Fig. 1). Stochastic perturbations may also result in ''stochastic resonance'': stochastic perturbations with a broad frequency spectrum can amplify oscillatory modes in the climate system, through the climate oscillation resonating with the noise at its own characteristic frequency (Stone et al. 1998).

Given the evidence from the ocean literature of the importance of idealized stochastic forcing in simulating and predicting ENSO, it is of interest to evaluate whether including a physically motivated stochastic

TABLE 1. Coupled and uncoupled integrations in CAM4.

Integrations	Duration	Forcing	Ensemble size
Coupled			
CTRL	1870–2004	Historical	1
SPPT	1870–2004	Historical	1
CTRL-1300	1–1300	Fixed 1850	1
Uncoupled			
CTRL	1979–2009	Historical	6
SPPT	1979–2009	Historical	1

parameterization scheme within a coupled GCM could improve the representation of ENSO in that model. In section 2, we consider the impact of the multiplicative stochastically perturbed parameterization tendencies (SPPT) scheme, which is widely used in the short- and medium-range forecasting community, in simulations with the National Center for Atmospheric Research (NCAR) Community Atmosphere Model (CAM) coupled to an ocean model. The results are presented in section 3. To help interpret the results, we then consider the impact of stochastic forcing in a simple delayed oscillator model for ENSO, which is presented in section 4. In light of these results, the results from CAM are analyzed in section 5 with a particular focus on the degree to which the coupling between atmosphere and ocean plays a role, before conclusions are drawn in section 6.

2. Stochastic parameterization in a coupled GCM

a. Model description and experiments

We begin by considering the impact of a stochastic parameterization scheme (SPPT scheme) on the representation of ENSO in a GCM. The integrations analyzed in this study use CAM, version 4 (CAM4; Gent et al. 2011), at a resolution of 0.9° × 1.25° with 26 vertical levels and a finite-volume dynamical core. Unless explicitly stated otherwise, all integrations use observed carbon dioxide concentrations in the atmosphere. The integrations are summarized in Table 1.

Two sets of experiments are performed. The first set consists of coupled simulations, whereby CAM4 is coupled to the NCAR ocean model, Parallel Ocean Program, version 2 (POP2; Danabasoglu et al. 2012), at 1° resolution with 40 levels in the vertical. It is also actively coupled to the Community Ice Code, version 4 (CICE4; Hunke and Lipscomb 2008), at 1° resolution and the Community Land Model, version 4 (CLM4; Lawrence et al. 2011). The atmosphere model is run with a time step of 30 min and communicates with the land and sea ice components at every time step, while the coupling with the ocean model is once per day (Gent et al. 2011). The coupled integrations cover the period 1870–2004 (135 years) and consist of an integration with the SPPT scheme and a control (CTRL) integration with no stochastic physics (see section 2b for a description of the SPPT scheme). In addition, a 1300-yr control (CTRL-1300) integration with fixed 1850s carbon dioxide forcing is available for analysis; this integration will be used to indicate the internal variability to be expected in coupled integrations with CAM4.

For comparison, we also perform a set of uncoupled simulations, whereby CAM4 is coupled to the active CLM4 and is prescribed sea ice from CICE4 and historical sea surface temperature (SST) reanalysis data from the Hadley Centre Sea Ice and SST dataset (HadISST). These integrations cover the period 1979–2009 (31 years). In one integration the SPPT scheme is used, and an additional six control integrations were available in which no stochastic scheme is used. The ensemble is generated by applying random perturbations of round-off magnitude to the atmospheric temperature field and indicates the degree of internal variability to be expected in CAM4. These six integrations were combined to give overall estimates of climate mean and variability for the control case. The model integrations are compared to observational and reanalysis datasets, detailed in Table 2.

b. The stochastically perturbed parameterization tendencies scheme

The stochastic scheme considered here is SPPT scheme (Buizza et al. 1999; Palmer et al. 2009), which was developed and is used operationally at the European Centre for Medium-Range Weather Forecasts (ECMWF). It has

TABLE 2. Observational and reanalysis datasets used in this study. (MLOST is the Merged Land–Ocean Surface Temperature analysis.)

Variable	Dataset	Period	Reference
SST	HadISST	1880–2011	Rayner et al. (2003)
Sea level pressure (PSL)	20CR, version 2	1880–2011	Compo et al. (2011)
Atmospheric surface (2 m) temperature (TAS)	MLOST	1880–2011	Vose et al. (2012)
Precipitation (PR)	GPCP	1979–2012	Huffman et al. (2009)
Zonal wind (U)	ERA-Interim	1979–2010	Dee et al. (2011)
Meridional wind (V)	ERA-Interim	1979–2010	Dee et al. (2011)
Vertical velocity (OMEGA)	ERA-Interim	1979–2010	Dee et al. (2011)
Cloud cover (CLDTOT)	ERA-Interim	1979–2010	Dee et al. (2011)

been adapted for operational use at the Met Office, Météo France, and the Japan Meteorological Agency, and testing is under way in the Consortium for Small-Scale Modeling (COSMO) model.

The scheme represents random errors associated with model uncertainty resulting from the model's physical parameterization schemes. A deterministic parameterization scheme aims to represent the average of the possible effects of the subgrid scale on the resolved-scale state. The SPPT scheme explores the impact of a range of potential realizations of the subgrid-scale processes by perturbing the deterministic parameterization tendency.

The SPPT scheme multiplies the tendencies from parameterized processes by a random number:

$$T = \frac{\partial X}{\partial t} = D + K + (1 + e)\sum_i P_i, \qquad (1)$$

where T is the total tendency in variable X. The term D is the tendency from the dynamics, K is horizontal diffusion, P_i is the tendency from the ith physics scheme, and e is the Gaussian distributed zero-mean random perturbation. The scheme perturbs the tendency for four variables: temperature T, zonal and meridional wind U and V, respectively, and humidity q. Each variable is perturbed using the same random number field, generated using a spectral pattern generator that evolves in time following a first-order autoregressive [AR(1)] process (Berner et al. 2009, 2015). The version of the SPPT scheme used here is a simplification of that described in Palmer et al. (2009); in this work, a single spectral pattern is used with a horizontal decorrelation scale of 500 km and a temporal decorrelation of 6 h. Different from the original implementation, the perturbation is not tapered close to the surface and in the stratosphere (Palmer et al. 2009).

c. *Significance testing*

It is important to gauge the statistical significance of the impact of this scheme. However, because of natural variability, different time slices from a single integration could have very different statistics, and even long samples on the order of a few hundred years can show significant variability in terms of mean and variance of fields. In light of this, we will use the CTRL-1300 run to estimate the significance of the observed difference between CTRL and stochastic model climates. The CTRL-1300 run is cut into nonoverlapping segments, each 135 years long. The diagnostic of interest is evaluated for each segment. If the difference between the stochastic and CTRL run is greater than half the range in diagnostics from the CTRL-1300 segments, the difference is said to be significant and is indicated by stippling on the figures. This makes the assumption that, while the mean climate does change if historical CO_2 forcing is accounted for, the climate variability does not change (Kay et al. 2015).

3. Results: Impact on El Niño–Southern Oscillation

The representation of ENSO in CAM4 has systematic deficiencies in both amplitude and temporal variability, as is typical for coupled models (Flato et al. 2013), although its spatial structure is greatly improved from earlier versions of the model as a result of improvements in convective parameterization (Neale et al. 2008). The state of ENSO can be diagnosed by constructing a time series of average SST in the Niño-3.4 region spanning from 170°W to 120°W and from 5°N to 5°S; a year is classified as being El Niño (La Niña) if the November–January seasonal average of the Niño-3.4 time series is more than one standard deviation above (below) the monthly mean.

Figure 1 shows the December–February (DJF) El Niño and La Niña spatial composites, which have been created by averaging model output from all years classed as El Niño or La Niña according to that model's Niño-3.4 time series.[1] Over ocean (land), the colors indicate the average SST [surface air temperature (TAS)] anomaly for El Niño or La Niña years, while the contours indicate sea level pressure anomalies. Figure 1c indicates that the CTRL run captures the spatial structure of the observed El Niño anomalies well, shown in Fig. 1a, both in terms of extent and width of warm tongue. The SPPT integration, shown in Fig. 1e, also captures the structure well. However, the CTRL run anomaly is too large compared to observations, which has been somewhat corrected for by SPPT. Figure 1d indicates that the CTRL run also largely captures the spatial structure of the La Niña anomalies, although the cold anomalies are too confined to low latitudes and do not extend far enough north. The CTRL anomalies are more than a degree too cold near the equator. The SPPT run has improved the magnitude of the cold SST anomalies during a La Niña event, as shown in Fig. 1f, as well as the spatial extent of the anomalies. Table 3 quantifies this improvement by calculating the pattern correlation (PC) and root-mean-square error (RMSE) between the observations and model simulations. While the PC gives a mixed picture as to which model is better, with the SPPT run outperforming CTRL for La Niña and vice versa, the RMSE indicates that the SPPT run outperforms CTRL for both phases of ENSO. The primary

[1] Many figures in this manuscript were made using code based on the NCAR Climate Analysis Section's climate variability diagnostics package (CVDP; Phillips et al. 2014).

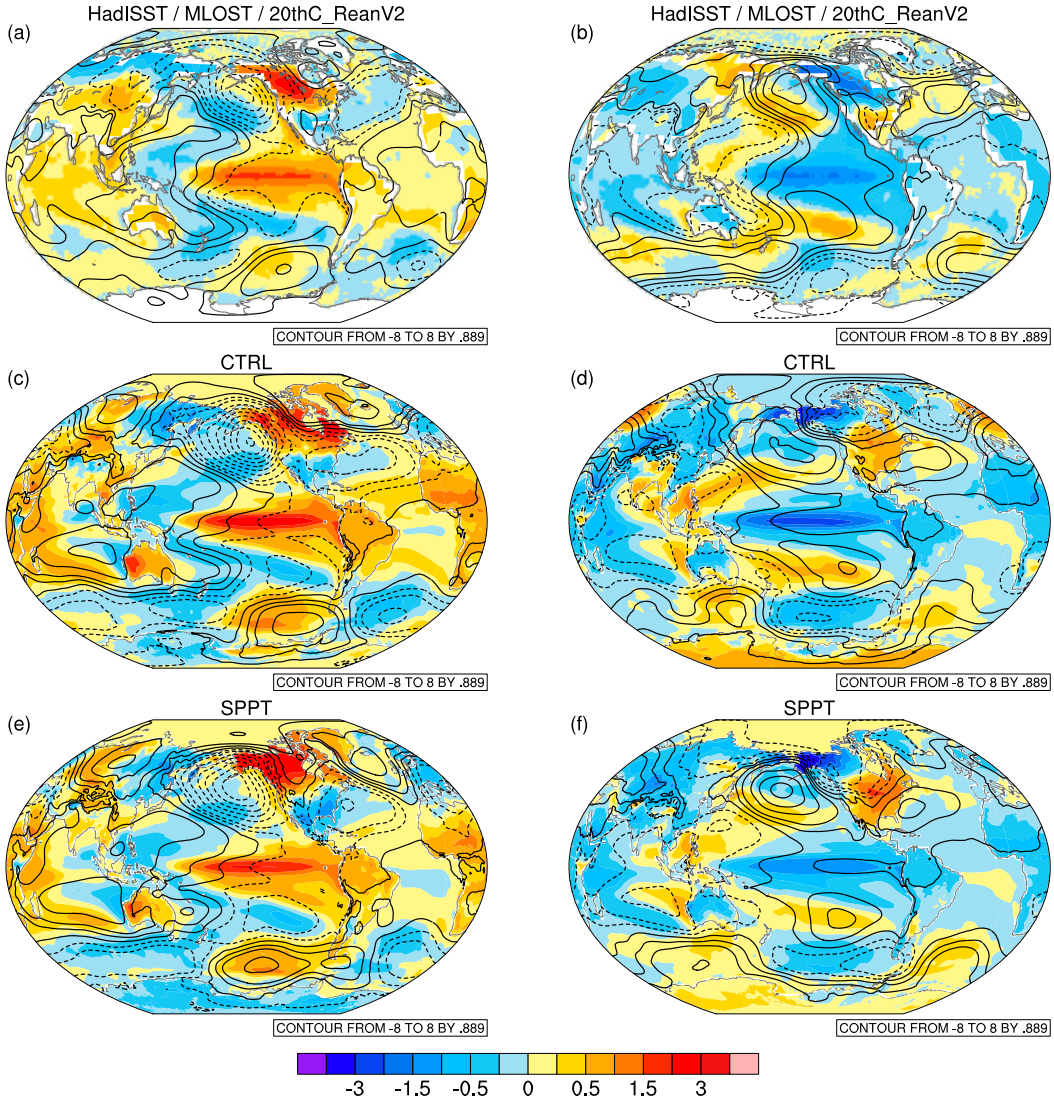

FIG. 1. (left) El Niño and (right) La Niña spatial composite for (a),(b) observations, (c),(d) CTRL, and (e),(f) SPPT. El Niño (La Niña) years are defined as years in the December Niño-3.4 time series greater than one standard deviation above (below) the mean. The colors indicate the SST anomaly (TAS anomaly over land; °C), while the contours indicate surface pressure anomalies (hPa).

impact of SPPT is in improving the magnitude of ENSO, not improving its spatial structure.

The improvement in the magnitude of La Niña but not El Niño indicates a change in skewness of the Niño-3.4 time series in the SPPT integration. While the observational Niño-3.4 data are positively skewed with a skewness of 0.26, the CTRL time series has a lower skewness of just 0.15. SPPT integration increases the skewness to 0.17.

The variability of ENSO in model and observations can be diagnosed using the Niño-3.4 time series. Figure 2a shows the monthly amplitude of the Niño-3.4 time series diagnosed from observations. The variability is at a maximum during boreal winter and a minimum during May and June. Figure 2b shows the amplitude for the CTRL run; the amplitude is approximately 40% too large at all times of year. Figure 2c shows that the SPPT scheme significantly reduces the amplitude of the Niño-3.4 time series at all times of year. The amplitude of ENSO in the SPPT run is a good match to observations, although it remains slightly too high in boreal summer.

The temporal variability of ENSO can be studied by considering the power spectrum of the Niño-3.4 time series. This is shown in Fig. 3. Figure 3b shows the CTRL spectrum (black) compared to the observational spectrum (gray). Typical of CMIP5 coupled models, the CTRL spectrum is too sharp, indicating that ENSO is excessively

TABLE 3. PC and RMSE between model runs and observations. The statistics summarize the results shown in the figures and indicated in the table. Boldface text highlights the better model for each variable for each diagnostic compared to observations if the difference is significant. The Pacific region is defined as 20°S–20°N, 80°–280°E.

Variable	PC			RMSE		
	CTRL	SPPT	Std dev	CTRL	SPPT	Std dev
Coupled runs						
El Niño SST (Global; Fig. 1)	**0.8655**	0.8297	—	0.1987	**0.1710**	—
La Niña SST (Global; Fig. 1)	0.7539	**0.8115**	—	0.2250	**0.1558**	—
El Niño PSL (Global; Fig. 1)	**0.7944**	0.6791	—	0.6282	**0.6149**	—
La Niña PSL (Global; Fig. 1)	0.5502	**0.5265**	—	0.5419	**0.5114**	—
U850 variance (Pacific; Fig. 6)	0.9083	0.8970	0.0061	0.4207	**0.2558**	0.0445
SST variance (Pacific; Fig. 7)	**0.8626**	0.8432	0.0090	0.1262	**0.0841**	0.0150
PR variance (Pacific; Fig. 8)	**0.8348**	0.8112	0.0039	0.3141	**0.2761**	0.0148
El Niño PR (Pacific; Fig. 9)	**0.8073**	0.7656	—	1.3993	**1.3743**	—
La Niña PR (Pacific; Fig. 9)	0.5973	**0.6099**	—	1.4938	**1.2761**	—
El Niño wind (Pacific; Fig. 10)	**0.8420**	0.7610	—	1.4838	**1.1208**	—
La Niña wind (Pacific; Fig. 10)	**0.7067**	0.6287	—	0.8973	**0.7220**	—
Uncoupled runs						
U850 variance (Pacific; Fig. 6)	**0.9205**	0.8965	0.0050	0.3457	**0.2725**	0.0122
PR variance (Pacific; Fig. 8)	0.8106	0.7986	0.0121	0.3770	0.3962	0.0142

periodic with dominant frequencies at 3 and 4 yr (Flato et al. 2013). This periodicity is not seen in observations (Fig. 3a), where power is more evenly distributed across frequencies. The observed spectrum shows less power in the ENSO signal compared to the CTRL run, as observed in Fig. 2. SPPT run has resulted in a large improvement in the temporal variability of ENSO; the amount of power in 3- and 4-yr oscillations is significantly reduced, and the power in higher-frequency oscillations, with periods less than 3 yr, has increased. There is also an improvement in the decadal variability of ENSO. The resultant spectrum is a good match to that observed.

The impact of a second stochastic scheme, the stochastic kinetic energy backscatter (SKEB) scheme (Shutts 2005; Berner et al. 2009), was also considered. The SKEB scheme is an additive scheme, which represents the upscale transfer of kinetic energy observed in the atmosphere by randomly perturbing the streamfunction, thereby injecting kinetic energy into the large scales in the model. Including this scheme in CAM4 had a very small impact on ENSO, both in terms of its spatial and temporal variability, so the results are not shown here. The impact of SKEB on the mean climate and other modes of atmospheric variability will be described in a future paper.

4. Stochastic parameterization in a DO ENSO model

It is important to understand the observed impacts of the SPPT scheme in CAM4. For example, it is surprising that the multiplicative SPPT scheme leads to a reduction in the magnitude of ENSO in CAM, whereas naïvely one would expect a stochastic parameterization scheme to enhance the variability of a GCM. It is not unprecedented for a multiplicative stochastic forcing to result in a damping that leads to a reduction in variance; other authors have discussed this counterintuitive effect from a theoretical perspective (Sardeshmukh et al. 2001, 2003) and in the context of a low-resolution medium-range forecasting model (Sardeshmukh 2005). When it comes to ENSO, it is of interest whether this damping is a general result or if it is specific to CAM4. To assist in the interpretation of results described in section 3, we first turn our attention to a much simpler model of ENSO—namely, a DO model (Suarez and Schopf 1988). This model shares many of the spurious characteristics of CAM4, having an overly periodic ENSO, so it is a suitable simple test bed for comparison with CAM4.

a. Model description

The DO model used in this study is taken from Stone et al. (1998). The one-dimensional (1D) model describes the evolution of eastern Pacific thermocline depth anomaly $h(t)$ with time (see the appendix for details). A white stochastic additive forcing with amplitude D_a relative to the seasonal cycle is applied to the equation describing the rate of change of thermocline depth anomaly. A multiplicative forcing is also considered; the parameter determining the strength of the ocean–atmosphere coupling κ is multiplied by a stochastic term to represent the impact of multiplicative noise in the atmosphere—for example, increased variability in westerly wind with increasing mean wind speed. This stochastic perturbation has relative amplitude D_m.

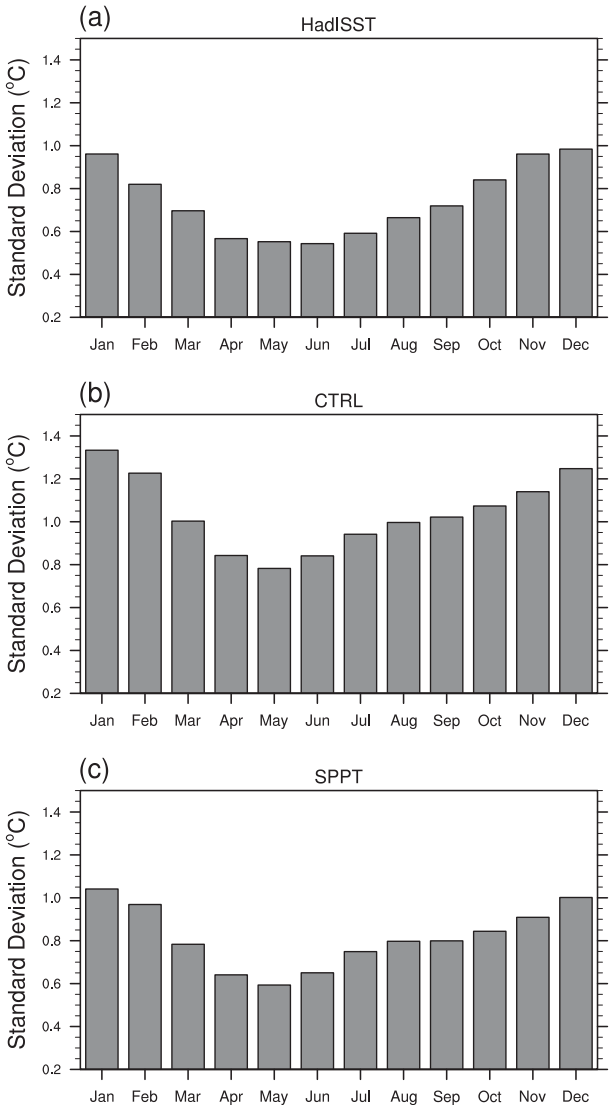

FIG. 2. Annual cycle in Niño-3.4 variability as demonstrated by the standard deviation of the monthly means of the Niño-3.4 time series in the coupled integrations: (a) observations, (b) CTRL, and (c) SPPT.

The system undergoes a Hopf bifurcation as κ is increased. For low values of κ the DO model does not undergo ENSO-like oscillations; only the annual cycle is present. If κ is increased above 1.335 an ENSO-like oscillation spontaneously emerges. Increasing the coupling parameter further results in larger-amplitude oscillations, as the coupled ocean–atmosphere system responds more strongly to perturbations in the system. It is illustrative to think of phenomena in the real ocean–atmosphere system using this framework. For example, in a minimal primitive equation model, the Atlantic multidecadal oscillation can arise through a Hopf bifurcation (Frankcombe et al. 2010). Indeed, intermediate-complexity models for ENSO, such as the Zebiak–Cane (ZC) model (Zebiak and Cane 1987) or the model described in Neelin (1990), undergo a bifurcation when the ocean–atmosphere coupling strength μ crosses a critical value μ_c (Roulston and Neelin 2000). In the ZC model, additive noise representing variability in wind stress is able to excite oscillations below μ_c (Roulston and Neelin 2000). The same behavior is observed in the DO model (Stone et al. 1998), which is therefore a useful tool within the hierarchy of models for understanding the impact of noise on ENSO. Furthermore, as indicated earlier, this particular ENSO model exhibits similar deficiencies to those in CAM4, so it could provide insight into the impact of stochastic parameterizations in the coupled GCM.

b. *Impact of stochastic noise*

The impact of additive and multiplicative noise on the DO model is considered in turn. For the additive noise case, D_m is set to zero and κ set to 1.4, and the D_a parameter is increased from 0 to 0.4225; for each value of D_a a 10 000-yr integration is performed. Figure 4c shows a sample of the time series for $D_a = 0.25$. The system begins to exhibit a regime-like behavior, moving between enhanced, large-amplitude oscillations and quiescent regions (Stone et al. 1998). The standard deviation of the smoothed time series is given as a function of D_a in Fig. 5a. Despite the increase in the quiescent regime, the variability of the system increases as the noise standard deviation increases in a number of discrete jumps. This is in contrast to the impact of the SPPT scheme in CAM4, where noise results in a reduction in variability in the system.

In the same way, the impact of multiplicative noise is considered. With D_a set to zero, the magnitude of multiplicative noise D_a is increased from 0 to 400, and a 10 000-yr integration is performed for each value of D_m.[2] Figure 4h shows a sample of the time series for $D_m = 36$. As the magnitude of multiplicative noise is increased, the oscillations become less regular. The standard deviation of the smoothed time series is given as a function of D_m in Fig. 5b. As for the additive noise case, the change in standard deviation takes place in a number of discrete jumps. However, unlike for the additive case, the system first shows a decrease in variability on including multiplicative noise, before increasing for large-magnitude noise. It is interesting, and important for the results presented in section 3, that even in a simple model including noise in

[2] Large amplitudes are required for D_m to achieve an appreciable change in κ_s when compared to κ. For example, setting D_m to 100 results in a standard deviation in κ_s of 0.65.

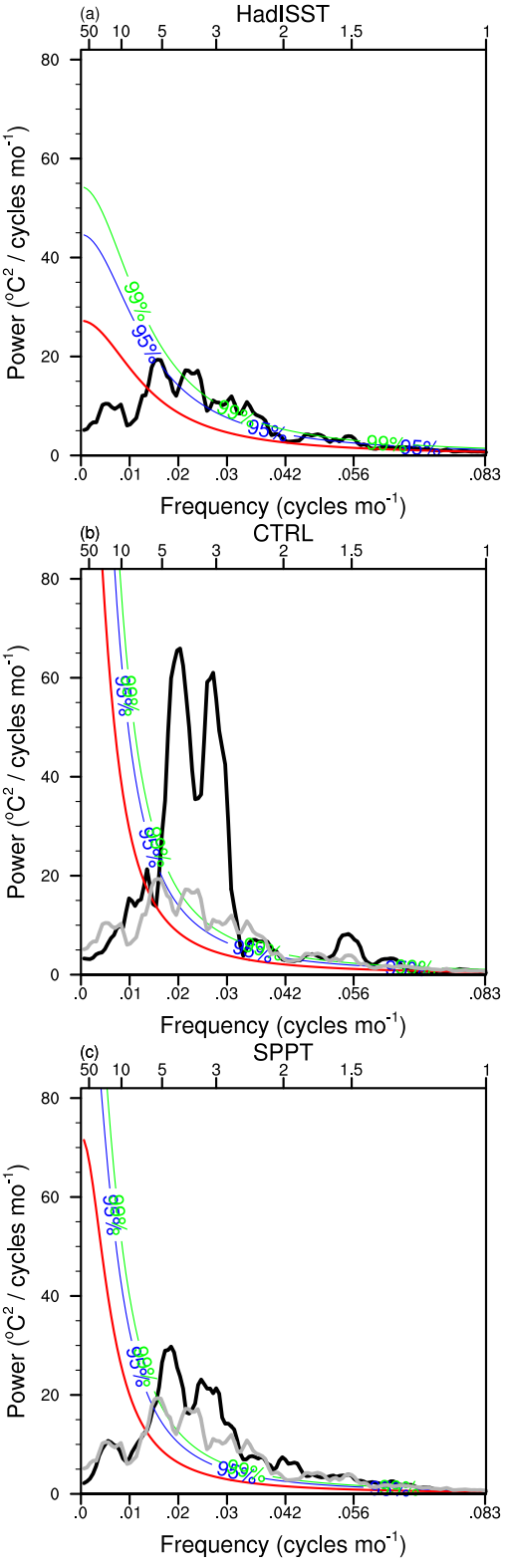

FIG. 3. Power spectrum of Niño-3.4 time series (black): (a) observations, (b) CTRL, and (c) SPPT. Also shown are the best-fit AR(1) spectrum (red) and its 95% and 99% confidence bounds (blue and green curves, respectively). The top x axis indicates the period in years, whereas the bottom x axis indicates the frequency in cycles per month. In (b),(c), the observational spectrum is shown in gray.

the system does not necessarily lead to an increase in variability.

For some periods, as seen in Fig. 4h, the system exhibits oscillations with a similar magnitude to the zero-noise case, but in general the multiplicative noise acts to damp the oscillations in the system. Since white noise is used to perturb the system, the system effectively sees a different coupling parameter κ every half-day. For moderate noise, the curvature of the Hopf bifurcation diagram means that negative perturbations have a larger impact on the expected amplitude of oscillations than positive perturbations, which could explain the reduction in amplitude. However, for large enough values of D_m, the perturbation can change the stability of the fixed point (FP) at each time step; large negative perturbations lead to a stabilization of the FP, while positive perturbations render it more unstable. The amplitude of oscillations is observed to increase; positive perturbations are now large enough for the system to enter the chaotic regime with large-magnitude ENSO oscillations, whereas the impact of large negative perturbations is limited to rendering the system stable (i.e., all $\kappa \leq 1.335$). In general, the multiplicative noise has altered the attractor of the system.

To understand the interaction between the noise and the DO model, wavelet decomposition is used to analyze the frequencies present in the DO time series and the time series of the applied additive and multiplicative noise (see the appendix for details). For all figures, the significance of the decomposition is indicated by the black contour, which indicates the time series has significantly different time–frequency characteristics than an AR(1) process at the 5% level.

Figure 4b shows the continuous wavelet transform (CWT) for the DO model without noise. There is significant power in the 2–4-yr-period band, with the peak in power at 3 yr. Figures 4d and 4i show the CWT for the additive and multiplicative noise forced DO time series, respectively, and Figs. 4e,j show the applied stochastic forcing in each case. For both the additive and multiplicative DO system, the oscillations are less regular than the zero-noise case, with power at a wider range of frequencies, although the underlying dominant frequency band remains the same. Figures 4e,j indicate that the stochastic forcing has power at a range of frequencies, with no single frequency dominating, as expected for white noise.

Figures 4g and 4l show the amplitude and phase of the wavelet coherence for the additive and multiplicative cases, respectively, which indicate regions of phase locking. For both cases, there are times when there is coherency between noise and model for oscillations with the characteristic period of 3 yr. For the additive case,

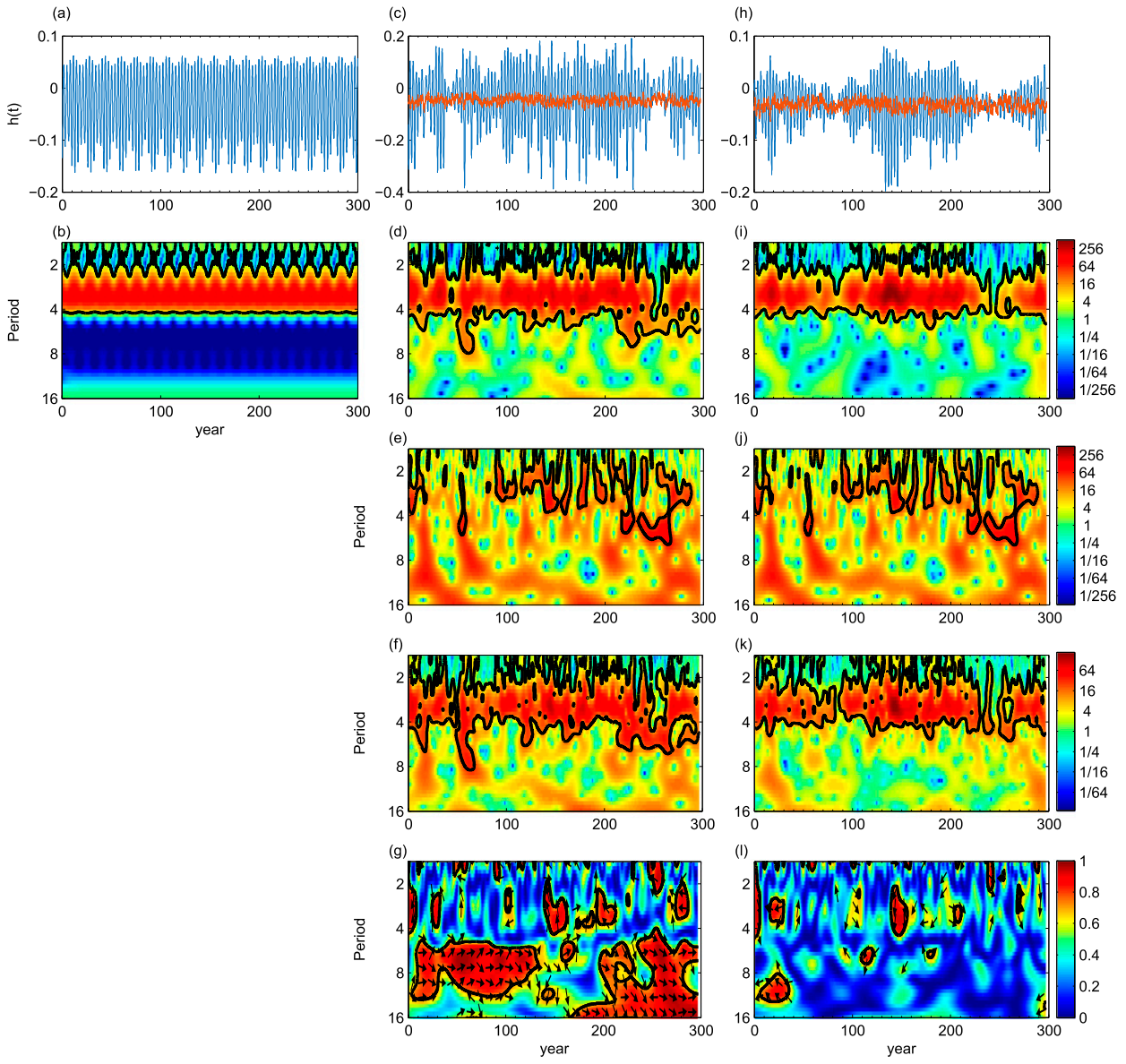

FIG. 4. Wavelet analysis applied to the DO model. Sample time series from the DO model with (a) no noise, (c) white additive noise with $D_a = 0.25$, and (h) white multiplicative noise with $D_m = 36$. The smoothed $h(t)$ time series is shown in blue, whereas the smoothed noise is shown in orange for (c),(h), vertically displaced to have the same mean as each $h(t)$ for ease of comparison. Continuous wavelet transform of (b) DO time series with no noise, (d) DO time series with additive noise, (i) DO time series with multiplicative noise, (e) additive noise time series, and (j) multiplicative noise time series. Note that the additive and multiplicative noise forcings are identical; they are merely applied to the system differently—(e) and (j) are identical. Amplitude of wavelet cross spectrum between the DO time series and the applied noise term for (f) the additive noise case and (k) the multiplicative noise case. Amplitude and phase of the wavelet coherence between the DO time series and the applied noise term for (g) the additive noise case and (l) the multiplicative noise case. Arrows pointing left (right) indicate antiphase (in phase) oscillations, whereas arrows pointing up (down) indicate the noise leads (lags) the DO model by 90°. The color bars in (i),(j),(k),(l) also indicate the color scales in (b),(d),(e),(f),(g), respectively. For all panels, the black contour indicates the 5% significance level (see text for details).

the phase of the wavelet coherence indicates that the noise leads the DO oscillations by approximately 100°, or 300 days, while for the multiplicative case the noise lags the DO oscillations by approximately 100°, or 300 days.

For the additive case this is an example of stochastic resonance. By chance, the low-pass-filtered variations in stochastic forcing synchronize with the oscillations in the system, amplifying the ENSO signal. However, even if the frequency of the noise is less favorable, the ENSO

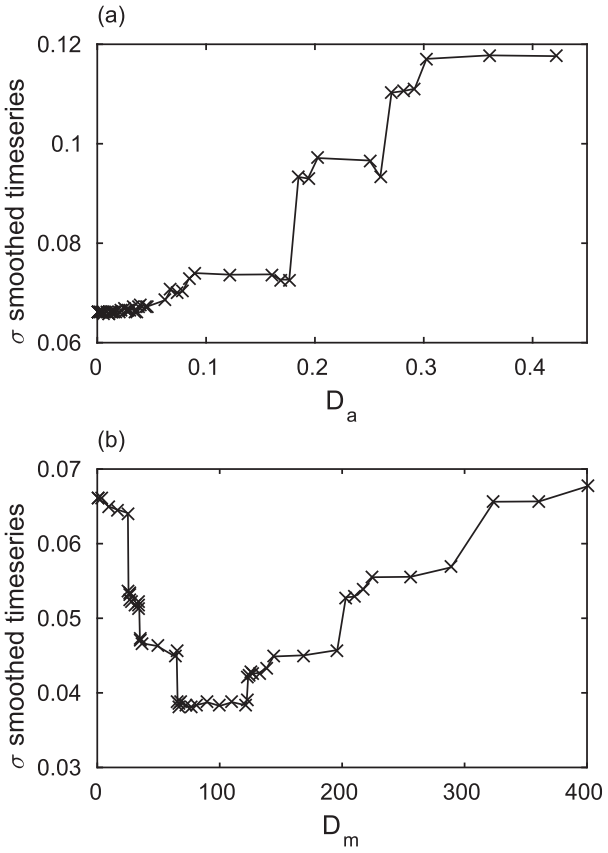

FIG. 5. Standard deviation of the DO time series as a function of magnitude of (a) additive noise and (b) multiplicative noise. The time series is first smoothed using a 12-month running average to remove the annual cycle.

system is still able to respond to the stochastic forcing. For example, the small ENSO event at year 250 in Fig. 4a has responded to the stochastic forcing, changing its frequency to match the slow variations in additive noise. Figure 4g also indicates high coherence at longer periods of 5 or more years.

For the multiplicative case, the ENSO signal can also be amplified if the low-frequency variations in stochastic forcing are in phase with the changes in thermocline depth. The system responds more strongly to this synchronization of the forcing frequency than in the additive noise case. When the low-pass-filtered variations in the stochastic term are not in phase with the oscillations of the system, the noise reduces the magnitude of the oscillations, while also introducing a richness of behavior into the oscillations. The ENSO system cannot respond so freely to the multiplicative stochastic forcing as to the additive—the stochastic forcing must work in unison with the oscillations of the system to amplify the oscillations and can only significantly impact the system at times when the thermocline forcing is large. For example, the system is unable to respond to the slow variations in stochastic forcing at year 250, and there is no coherency for low-frequency oscillations, unlike the additive case.

5. Understanding the impact of SPPT on ENSO

In light of the results from the DO model, we return to CAM, where we seek to understand the improvement in the amplitude and temporal characteristics of ENSO as a result of the SPPT scheme. The SPPT scheme only acts on the atmospheric components of the model with a short 6-h time scale, and it is not clear why perturbing the atmosphere in this way should positively impact the ENSO coupled system. Furthermore, it is not clear why the SPPT scheme should have such a large impact on ENSO, while the additive SKEB scheme has little impact—in the DO model, both additive and multiplicative noise altered the behavior of the system. Nevertheless, the fact that multiplicative noise also led to a reduction in variability in the simple DO model gives us confidence in the generality of this result in the context of the ENSO system—it is unlikely to be due to the specifics of the coupled CAM model.

There are several hypotheses for how SPPT could impact ENSO. The first is that the SPPT scheme directly results in improvements in the variability of one component of the ENSO system. In the coupled integrations, the improved variability in this component is able to improve the variability of the next aspect of the ENSO cycle and so on, ultimately amplifying the improvement in the first component through the coupled oscillation.

An alternative hypothesis is that the SPPT scheme systematically alters the coupling between the atmosphere and ocean. In the context of the deterministic DO model, reducing the strength of the coupling moves the system toward the Hopf bifurcation point, reducing the amplitude of the oscillation; the characteristic time scale of oscillation is unaltered, but the rate of perturbation growth has been reduced. An alternative, more subtle interaction of multiplicative noise with the coupling parameter can be motivated by our discussion in section 4. There it was suggested that multiplicative noise reduced the magnitude of oscillations in the system because of the shape of the bifurcation diagram; while the average value of the coupling parameter remains the same, negative perturbations to the coupling parameter have a larger impact on the magnitude of the oscillations than positive perturbations.

A third hypothesis is that SPPT could impact the initiation and termination mechanisms for El Niño and La Niña events. By increasing the probability of early termination of an event, the average amplitude of events

would decrease and large-amplitude events would be less likely (although still possible). This would also impact the temporal characteristics of the ENSO system, reducing the periodicity of the signal. This is equivalent to SPPT altering the shape of the bifurcation diagram—a given coupling parameter results in oscillations of smaller amplitude than in the CTRL integration.

a. The coupled system

To consider the first hypothesis, each component of the coupled ENSO system is considered in the atmosphere-only simulations. During an El Niño event, weakening of the easterly trade winds results in a relaxation of the thermocline, with warm water spreading eastward. Convection follows the warm waters, moving from the warm pool to the central Pacific. This movement of convection results in a reduction of surface pressure in the central Pacific and an increase in the west, impacting the Walker circulation, which exacerbates the weakening of the easterly trades. In the coupled integrations, improving one component of the system can impact the whole system through this feedback loop. However, in the atmosphere-only integrations, the coupling to the ocean does not exist, so there can be no oceanic response to a change in winds, breaking the feedback cycle.

Figure 6 shows the impact of SPPT on the annual mean variance of zonal wind at 850 hPa (U850) in the atmosphere-only and coupled integrations. In both the uncoupled and coupled control integrations (Figs. 6b and 6c, respectively), the annual mean wind field shows too much variability in the central and western tropical Pacific and Indian Oceans. The SPPT scheme coherently reduces the variability in annual mean zonal wind in both the atmosphere-only and coupled integrations in this region. Table 3 quantifies this improvement; the SPPT scheme significantly improves the RMSE of zonal wind variance for both the atmosphere-only and coupled simulations.

The variability of SST is shown in Fig. 7 for the coupled runs. The CTRL integration shows too much variability in SST in the tropical Pacific. The SPPT integration shows a reduction of variability across the equatorial Pacific, correcting the bias in variability in the CTRL run. This is consistent with the improved amplitude of El Niño and La Niña events observed in Fig. 1.

The variability of large-scale convection is diagnosed through considering precipitation, vertical motion, and cloud cover. Figure 8 shows the impact of SPPT on the variability of precipitation; the changes in variability of cloud cover and vertical motion are similar to those for precipitation, so they are not shown for brevity. For all these variables in the coupled runs, the SPPT scheme results in a coherent reduction in variability across the central tropical Pacific. However, no such signal is observed in the atmosphere-only integrations; the SPPT scheme has an impact, but it is not in the form of coherently reducing variability in the tropical Pacific, as would indicate an improvement in the atmospheric component of ENSO commensurate with the improvement in wind variability. Table 3 indicates that the improvement in precipitation variability is significant in the coupled simulation according to the RMSE but that, as expected, there is no significant change in RMSE for the atmosphere-only simulations.

In contrast, for zonal wind, cloud cover, vertical velocity, and precipitation, the SPPT scheme has only a small impact on the mean in both coupled and atmosphere-only integrations (not shown)—the largest effect is an improvement in variability.

These results support the first hypothesis. The SPPT scheme initially improves the variability of zonal wind in CAM. In the coupled integrations, this improvement in zonal wind impacts the ocean, improving the variation of SST, which in turn improves the modeled convective variability. In all cases, the SPPT scheme reduces the strength of the mean anomalies in these variables, reducing the amplitude of ENSO in the model. In the atmosphere-only integrations, there is no oceanic response to improved zonal wind anomalies, so no response is observed in convection.

The magnitude of zonal surface wind in the tropical Pacific is set by two processes, upper-level forcing and boundary layer processes (Chiang et al. 2001); one of these processes alone is unable to sustain the anomalous convergence (Wu et al. 1999). Upper-level forcing is provided by anomalous heating from convection, while boundary layer processes are dominated by SST-induced boundary layer convergence. In the atmosphere-only integrations, it is unlikely that an improvement in boundary layer processes could drive the observed improvement in zonal wind since the integrations have the same prescribed SST. This points to anomalous convective heating as the source of the observed improvement.

The SPPT scheme perturbs the convective heating tendencies, but the perturbation is symmetric and so directly results in neither a net increase nor reduction in convective heating. The anomalous heating from convection is due to anomalous precipitation from deep convective clouds (Sarachik and Cane 2010). While the SPPT scheme does not directly perturb precipitation, it can impact precipitation at future time steps through its perturbation of the deep convective temperature and humidity tendencies.

Consider regions of persistent, organized convection. A positive perturbation to the convective tendencies will

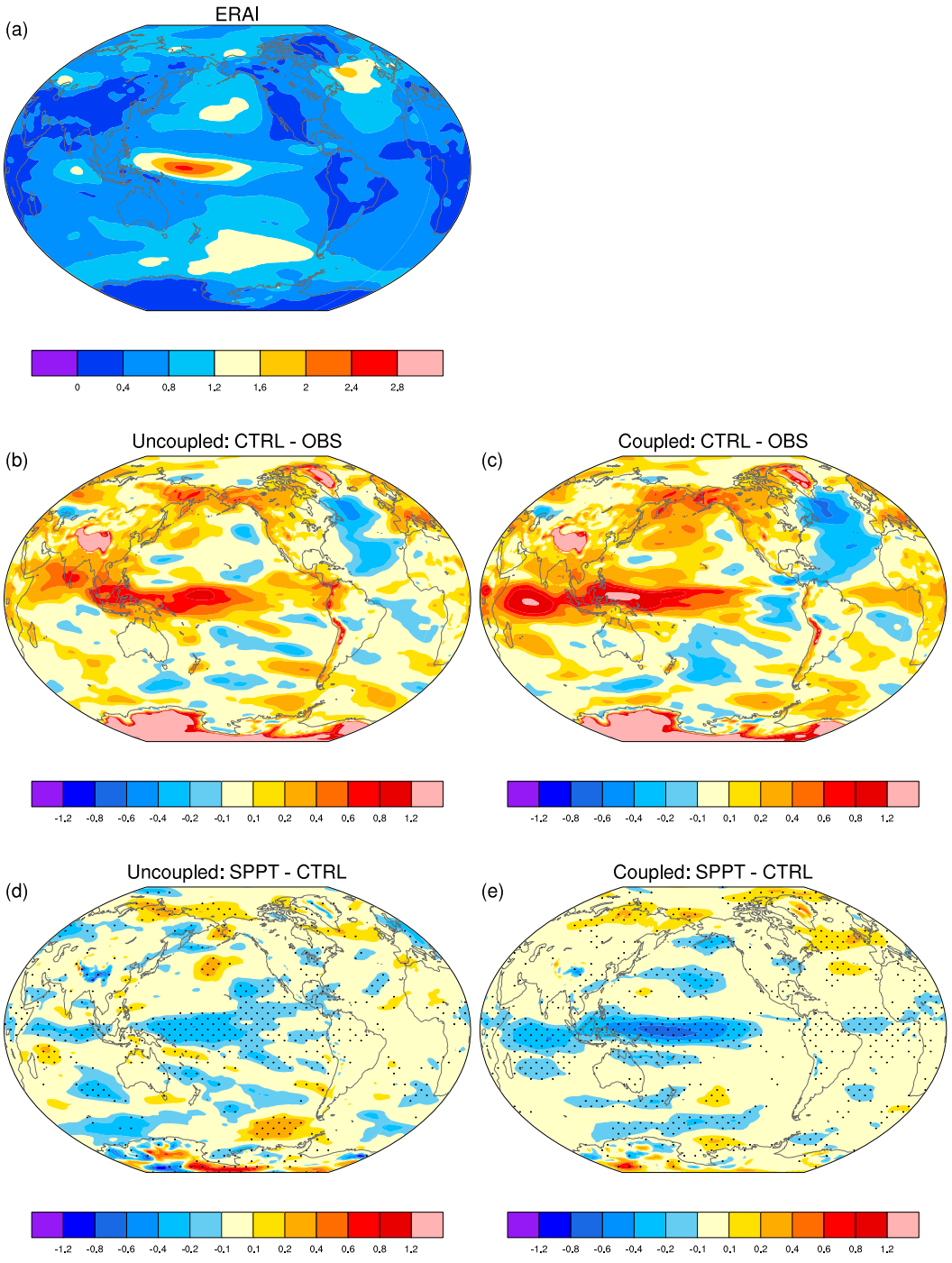

FIG. 6. (a) Variance of annually averaged zonal 850-hPa wind ($m^2 s^{-2}$) for observations (OBS). Bias in the variability of the control run CTRL − OBS, for (b) uncoupled and (c) coupled integrations and SPPT − CTRL, for (d) uncoupled and (e) coupled integrations.

mimic enhanced convection at that time step (without the associated enhanced precipitation). The resultant additional stabilization of the atmosphere will reduce convection and therefore convective precipitation at the next time step. A negative perturbation will have the opposite effect: less stabilization at the current time step will enhance convective precipitation and convective heating at the next time step. The situation is symmetrical, with neither a net increase nor decrease in convective precipitation or anomalous heating expected due to SPPT.

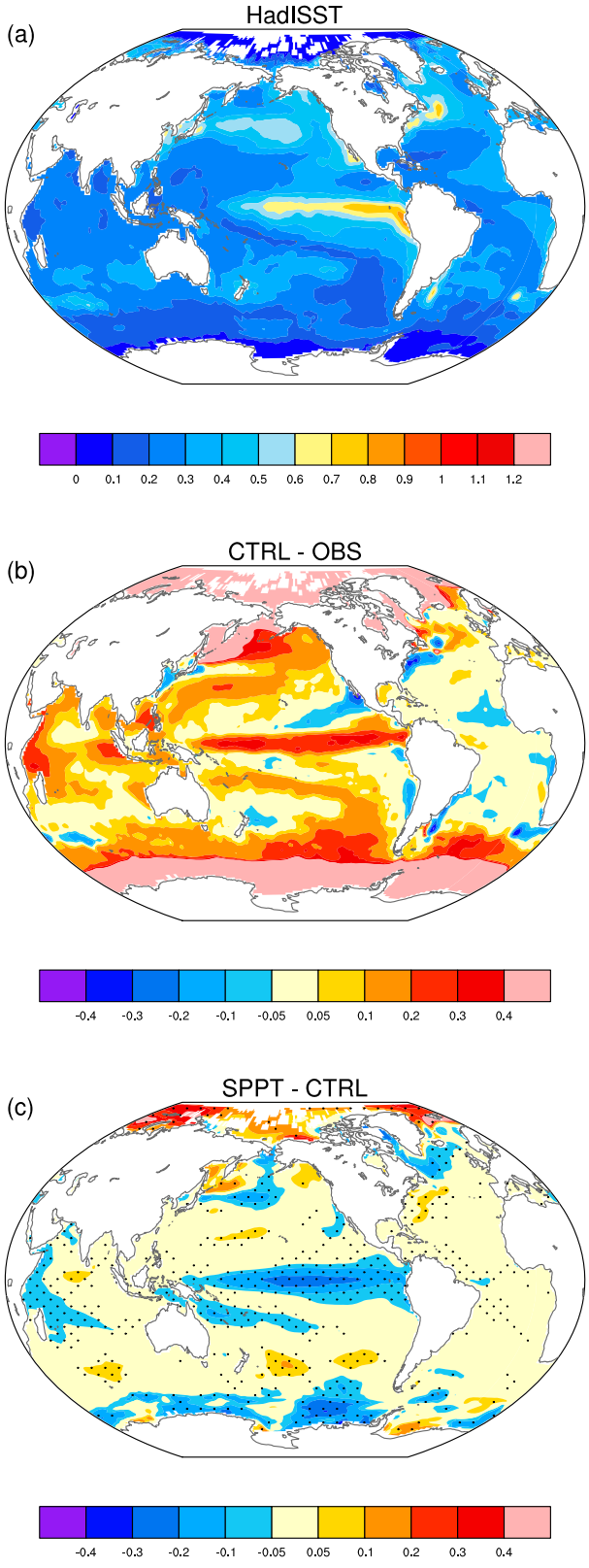

FIG. 7. Variance of annually averaged sea surface temperature ($°C^2$) for the coupled integrations: (a) OBS and (b) bias in the variability of the control run: CTRL − OBS and (c) SPPT − CTRL.

However, when regions with little convection are considered, an interesting nonlinearity is observed. As before, positive perturbations mimic enhanced convective activity at the previous time step, suppressing convection at later time steps further, while negative perturbations have the opposite effect. However, there is a limit to the effect of these perturbations in one direction: anomalous negative heating cannot exceed the negative of the climatological heating, as the amount of precipitation cannot be negative (Sarachik and Cane 2010). This asymmetry results in a net increase of precipitation in regions with suppressed convection. This reduces the anomalous cooling and the strength of the forcing, which leads to reduced divergence. It is likely this net increase in precipitation, while possible in both phases of ENSO, will be more dominant in the La Niña phase, where convection is suppressed in the central Pacific.

The importance of asymmetries in the convective response to a stochastic forcing has also been highlighted by Tompkins and Berner (2008), who consider the influence of symmetric zero-mean perturbations on convection. They find that positive perturbations trigger convection easily, leading to an increase in convective activity, while negative perturbations rarely affect convective events, leading to a strongly biased response.

To test the proposed mechanism, Fig. 9 shows the composite precipitation anomalies for El Niño (Figs. 9a,c,e) and La Niña (Figs. 9b,d,f) for the coupled integrations. Figures 9c,e show that the positive El Niño precipitation anomaly in the central-western Pacific is slightly increased for the SPPT integrations compared to the CTRL, although the slight reduction in precipitation anomaly in the central-eastern Pacific could indicate a shift in convection anomaly. In contrast, Figs. 9d,f show a significant reduction in the magnitude of the La Niña negative precipitation anomalies across the central Pacific. The resultant composite wind anomalies are shown in Fig. 10 for El Niño (Figs. 10a,c,e) and La Niña (Figs. 10b,d,f). As expected, the reduction in wind anomalies is greater for La Niña than for El Niño. Table 3 shows the PC and RMSE between models and observations: the SPPT scheme improves the RMSE for both variables in both phases.

The presence of this asymmetry in regions of suppressed convection, but not in regions of enhanced convection, results in a large reduction in the magnitude of La Niña events and a smaller impact on El Niño events. This is as observed in Fig. 1: the reduction in ENSO amplitude in the model is primarily due to a reduction in the amplitude of La Niña events. It is not the case that the SPPT scheme systematically alters the

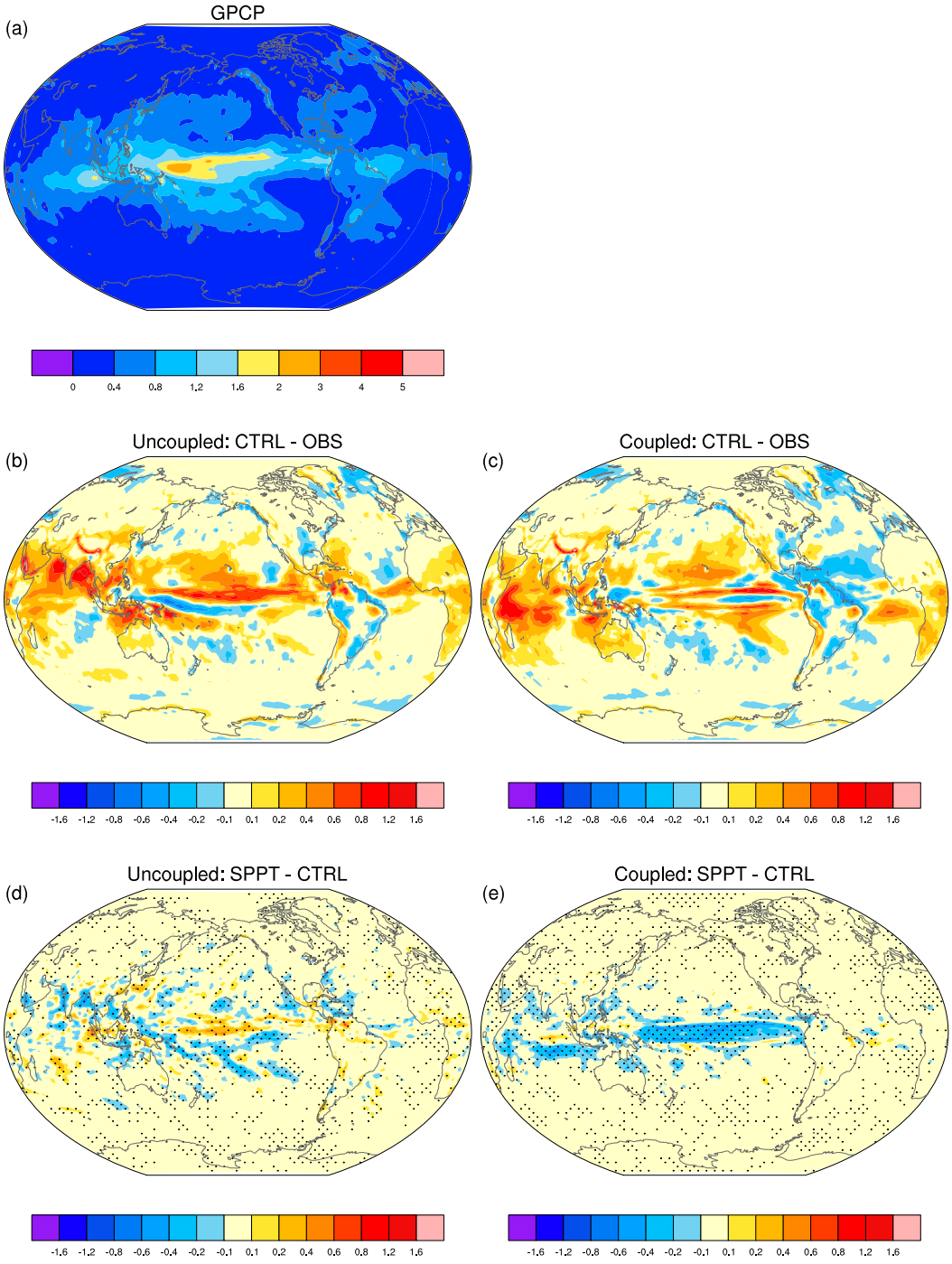

FIG. 8. (a) Variance of annually averaged precipitation ($mm^2\ day^{-2}$) for OBS. Bias in the variability of the control run CTRL − OBS, for (b) uncoupled and (c) coupled integrations, and SPPT − CTRL, for (d) uncoupled and (e) coupled integrations.

coupling between the atmosphere and ocean at all times, but rather it appears to effectively reduce the strength of the coupling parameter in the La Niña phase of ENSO—in the SPPT run, a given La Niña SST forcing anomaly results on average in a smaller convection anomaly than in the CTRL run. This bears similarities to the impact of multiplicative noise in the DO model as outlined in section 4; in that case, negative perturbations were able to suppress the system's response to a thermocline anomaly more effectively than positive perturbations

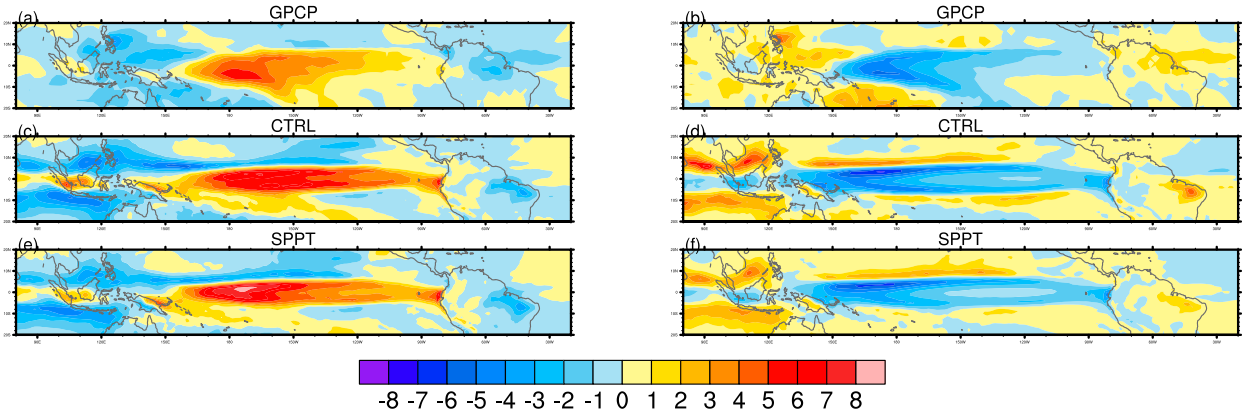

FIG. 9. (left) El Niño and (right) La Niña precipitation anomaly (mm day^{-1}) composites for DJF: (a),(b) OBS, (c),(d) CTRL, and (e),(f) SPPT. Anomalies are constructed as in Fig. 1.

amplified the response, which led to a systematic reduction in amplitude of the ENSO oscillation.

b. *Westerly wind bursts*

The results indicate that the SPPT scheme leads to a reduction of amplitude of cold events due to a reduced ocean–atmosphere coupling during La Niña. However, perhaps it could be possible to achieve a similar systematic result using a deterministic parameterization. Does SPPT also impact ENSO in a way that cannot be achieved using a deterministic parameterization scheme?

One possible mechanism which could lead to such an improvement is westerly wind bursts (WWBs). WWBs can be defined as spatially and temporally coherent westerly wind events in the equatorial Pacific with a wind speed greater than, for example, 7.0 m s^{-1} (Chen et al. 2015). It is known that WWBs act on top of a regular El Niño–La Niña cycle. Because they are orientated in a westerly direction, they strongly impact El Niño through the triggering of new El Niño events, but they do not directly impact La Niña. Atmospheric noise is thought to be the primary forcing for decadal variability in ENSO (Yeh and Kirtman 2006). In particular, the state-dependent nature of the stochastic WWB forcing is thought to be important (Jin et al. 2007; Levine and Jin 2010, 2015). In observations, the occurrence of WWBs is modulated by SST, but they also have a large stochastic component (Tziperman and Yu 2007).

To quantify the impact of SPPT on WWBs, we first consider Fig. 11a, which shows the PDF of daily westerly wind anomalies, where the time series are first smoothed using a 5-day running mean to highlight temporally persistent anomalies. The data are taken from the atmosphere-only integrations to remove the impact of SST changes on WWBs. It indicates that the CTRL integration has too many strong westerly wind anomalies compared to observations and that the SPPT scheme reduces the frequency of these large anomalies. Figure 11b shows an enlargement of Fig. 11a for wind

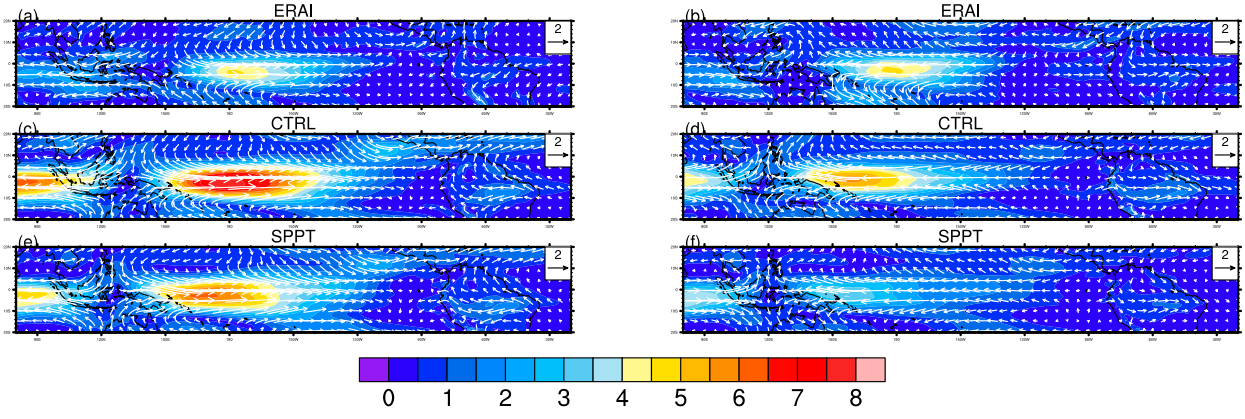

FIG. 10. (left) El Niño and (right) La Niña wind anomaly composites for DJF. Colors indicate anomalous wind speed (m s^{-1}), whereas arrows indicate anomalous wind direction: (a),(b) OBS, (c),(d) CTRL, and (e),(f) SPPT. Anomalies are constructed as in Fig. 1.

anomalies above $7\,\mathrm{m\,s^{-1}}$; while the CTRL and SPPT runs are similar for moderate wind anomalies between -5 and $7\,\mathrm{m\,s^{-1}}$, for large-amplitude anomalies, the SPPT scheme results in a large, statistically significant improvement toward observations.

We can further consider the impact of SPPT on WWB by considering the distribution of WWBs as a function of SST in the equatorial Pacific (5°N–5°S, 130°–260°E). Figure 12 shows the monthly averaged fractional area coverage of WWBs[3] as a function of time for the atmosphere-only integrations, compared to the fractional area of the Pacific warm pool, defined as regions with SST greater than 28.5°C.

While SST greater than 28.5°C is a good predictor of WWBs, they do not always occur—the presence of warm SST is a necessary but not sufficient condition for WWBs. The CTRL integration shows a stronger impact of SST on WWBs; warm SSTs very likely result in WWBs, resulting in more WWB events than in observations. The SPPT run results in an overall reduction in the number of WWBs, as indicated in Fig. 11, but on occasion it also triggers WWBs not observed in the CTRL run (e.g., late 1981 and early 1991). By perturbing the convective tendencies, the SPPT run is able to represent the stochastic component of WWBs. Note that, as required, the modulation of WWBs by SST is maintained by the SPPT scheme since convection tendencies are largest over warm waters, although warm SST now no longer guarantees a WWB.

The relationship between WWBs and SST can be quantified further by diagnosing the state dependency of the wind forcing on SST anomalies using monthly mean data for the coupled integrations. Following the analysis of Levine and Jin (2015), a time series of the monthly SST and U850 anomalies averaged over 3°S–3°N, 160°–200°E is formed. The wind anomaly is assumed to be the sum of a deterministic component and a state-dependent stochastic component, both functions of the SST anomaly:

$$U = U_D + U_S, \tag{2}$$

$$U_D = \mu_1 T + \mu_2 H(T) T + \mu_{\mathrm{AC}} T \cos(\omega_{\mathrm{AC}} t - t_{\mathrm{AC}}) + \mu_{\mathrm{SAC}} T \cos(\omega_{\mathrm{SAC}} t - t_{\mathrm{SAC}}), \quad \text{and} \tag{3}$$

$$U_S = \mu_S [1 + BH(T)T], \tag{4}$$

where U_D is the deterministic component of the wind, and U_S is the stochastic component. Note that this analysis assumes that the stochasticity does not cause any structural changes in the dynamical description of the system, as cross terms have been ignored in Eq. (2). The deterministic component is decomposed into a linear response to SST T, a threshold nonlinear response for temperature anomalies greater than zero using the Heaviside function $H(T)$, and combination tones in time t, arising from the interaction of ENSO with the annual cycle (AC) and semiannual cycle (SAC). The variables μ_1, μ_2, μ_{AC}, μ_{SAC}, ω_{AC}, ω_{SAC}, t_{AC}, and t_{SAC} are constants which characterize the deterministic component of the wind and should be fitted from the data. The stochastic component is state dependent and represents

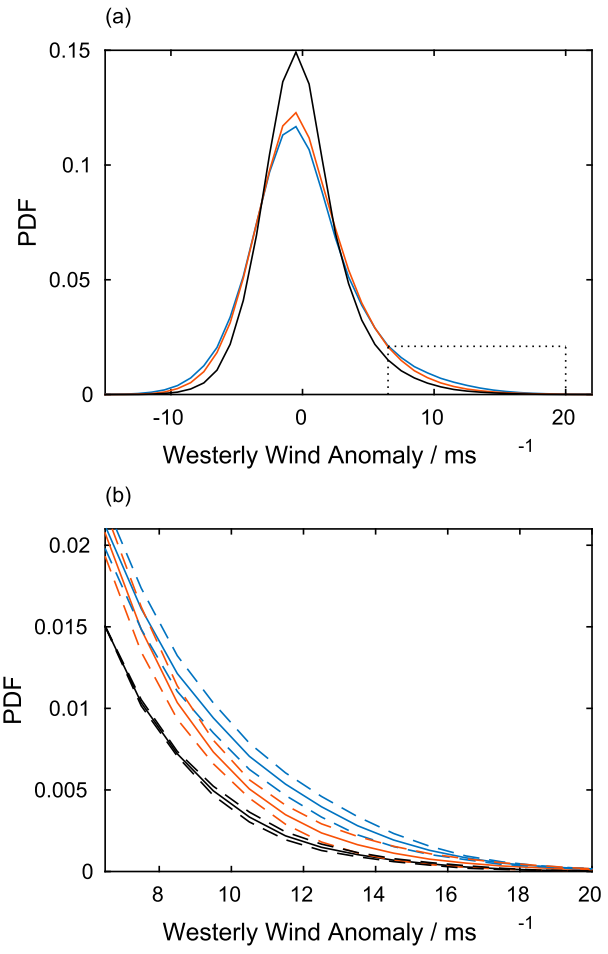

FIG. 11. Quantifying the impact of SPPT on the distribution of U850 (westerly wind) anomalies ($\mathrm{m\,s^{-1}}$). (a) Distribution of wind anomalies from the ERA-Interim dataset (black), CTRL (blue), and SPPT (red) model runs. The data are first smoothed using a 5-day running mean, and the PDFs are constructed using all spatial points between 5°N and 5°S and between 130° and 260°E. The region within the dotted box of (a) is enlarged in (b) to highlight the differences in the tail. The dashed lines indicate the same diagnostic evaluated for the first and second half of each dataset, respectively, to give an indication of the significance of the difference between the curves.

[3] Here, a spatial point is defined to have a WWB if the U850 zonal wind anomalies are greater than $7\,\mathrm{m\,s^{-1}}$, where the U850 time series is first smoothed using a 5-day running average to ensure temporal coherency.

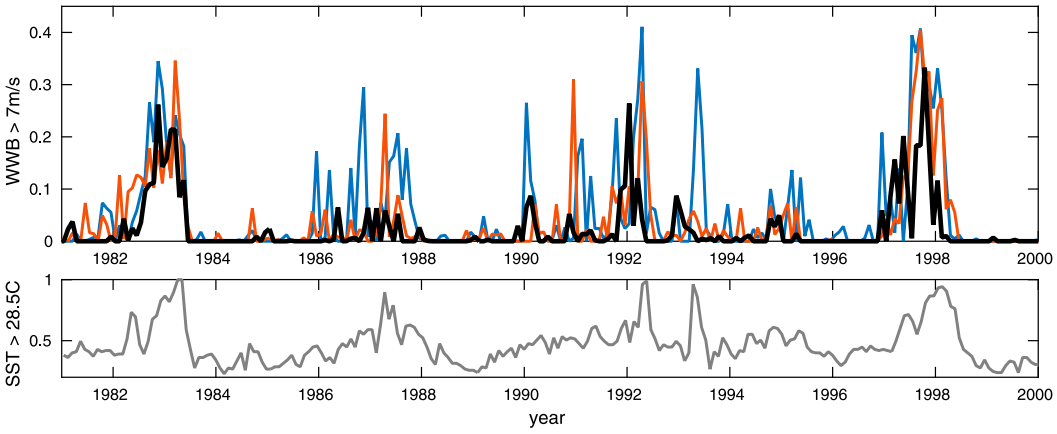

FIG. 12. (top) WWBs and (bottom) SST for the atmosphere-only integrations as a function of time for the ERA-Interim dataset (black), CTRL (blue), and SPPT (red) model runs. The time series show the monthly average fraction of grid points that show WWB $> 7\,\mathrm{m\,s^{-1}}$ in (a) and SST > 28.5°C in (b).

the increased likelihood of stochastic WWBs with enhanced SSTs. Of particular interest are the μ_1 and μ_2 parameters, which quantify the deterministic response of the wind to the SST anomalies, and the B parameter, which describes the degree of state dependence of the WWB forcing. The parameters are fitted following a similar methodology to Levine and Jin (2015) and are shown in Table 4. It was found that SPPT integration results in a reduction of these three parameters compared to the CTRL integration. The reduction in the deterministic response parameters reinforces the mechanism proposed in section 5a; the SPPT run results in a reduction in the strength of the coupling between ocean and atmosphere. The reduction in the degree of state dependence of the stochastic term confirms the conclusions drawn from Fig. 12—namely, that WWBs are too strongly coupled to SST in the CTRL run and that the SPPT run reduces this degree of dependency toward observations.

WWBs act as a stochastic forcing to the ENSO system. They may produce extreme El Niño events if the timing is right or can produce moderate central Pacific El Niño events. The interplay between the phase of the ENSO system and the timing of the multiplicative stochastic forcing is similar to that observed in the DO system: multiplicative noise can only amplify the ocean–atmosphere coupling (e.g., initiate new WWBs) if the timing is right and otherwise tends to damp the oscillations. Representing the stochastic nature of WWBs improves the temporal characteristics of ENSO, reducing the periodicity of the oscillation; in the CTRL run, warm SSTs predictably lead to WWBs, which lead to predictable initiation and ultimately termination of El Niños and an overly periodic power spectrum.

Other authors have found that the amplitude of ENSO in an intermediate-complexity coupled model can double if WWBs modulated by SST are imposed compared to a model where the stochastic WWB forcing is uncorrelated to SST (Eisenman et al. 2005). A different study in a simple ENSO recharge oscillator model also found that including state dependence in the stochastic forcing led to an increase of ENSO instability and amplitude (Jin et al. 2007; Levine and Jin 2010). Our results are consistent with these studies and demonstrate this mechanism at work in a fully coupled GCM. While it is important that WWBs are modulated by SST, the degree of modulation in the CTRL run is too strong. It is likely that reducing the correlation between WWBs and SST and increasing the stochastic component have contributed to the observed reduction in ENSO amplitude in the SPPT integrations.

6. Concluding remarks

Despite ongoing improvement in the deterministic parameterization schemes important for ENSO, models still exhibit large systematic errors in their representation of the climate mean and variability in the tropical Pacific. Since evidence from observations

TABLE 4. Parameters in Eq. (4) fitted to observations (OBS) and model data.

Parameter	OBS	CTRL	SPPT
μ_1	2.49	2.69	2.29
μ_2	0.40	0.54	0.30
μ_S	1.77	2.19	2.13
B	0.83	0.92	0.57
μ_{AC}	−0.92	−1.04	−0.49
μ_{SAC}	−0.37	0.09	0.08
t_{AC}	2.16	2.76	2.66
T_{SAC}	0.66	−0.14	−0.24

and modeling studies points to the importance of stochastic processes in forcing ENSO, we investigate the impact of including stochastic parameterization schemes on the representation of ENSO in a fully coupled GCM. We also consider a simple delayed oscillator (DO) model for ENSO as it exhibits similar deficiencies to the fully coupled GCM. In particular, both have an ENSO signal that is too periodic compared to observations.

The stochastically perturbed parameterization tendencies (SPPT) scheme developed at ECMWF was tested in coupled and uncoupled simulations with NCAR CAM4. This is a multiplicative noise scheme, which perturbs the total parameterized tendencies in temperature, horizontal winds, and humidity with a spatially and temporally correlated random number. In this way it represents the uncertainty in the tendencies associated with the parameterization process. Introducing SPPT into coupled simulations of CAM4 reduces the amplitude of ENSO; when compared to the control integration, the SPPT integration has variability that better matches observations. In the delayed oscillator model, additive noise was found to increase the variability of ENSO, whereas a multiplicative scheme led to a reduction in variability, reflecting the impact of SPPT in CAM4.

It is suggested that the observed reduction of variability in CAM4 is due to two mechanisms. First, the SPPT scheme results in an improvement (reduction) of variability in the zonal winds. This occurs through an asymmetric response of the model to the symmetric perturbation of the convective heating tendencies. This improvement in wind variability improves the variability in SST and tropical convection through the ENSO coupled system, ultimately feeding back to strengthen the improvement in the zonal winds. Second, the SPPT scheme improves the distribution of westerly wind bursts (WWBs) in the model, important for triggering El Niño events, by increasing the stochastic component of their variability and reducing their degree of state dependence on SST toward that observed.

Other studies have also shown the ability of stochastic forcing to reduce the amplitude of ENSO; Roulston and Neelin (2000) show that including a stochastic wind forcing term can reduce the variability in an intermediate coupled model. However, only additive noise was tested, and the reduction only occurred if the additive stochastic forcing was first filtered to leave only the high-frequency components. All other cases tested, including red noise and unfiltered white noise, resulted in an increase of variability (Roulston and Neelin 2000). This is consistent with our results in section 4, where white additive noise increased ENSO variability in the DO model. It is interesting that in our study, multiplicative noise is able to damp ENSO without the high-frequency bandpass filter. The multiplicative noise tested in the DO model was white, while the multiplicative noise in CAM is red—both contain significant low-frequency variability, and both damp ENSO. However, the wavelet analysis performed on the DO model indicates that the low-frequency variability in the stochastic forcing is unable to interact with the modeled ENSO. It is possible that the multiplicative nature of the noise effectively filters out the lower-frequency oscillations, as they are not effective in impacting the coupled oscillation. It is only the high-frequency forcing that can interact with, and stochastically damp, ENSO.

This brings us to a general result from both the DO and CAM experiments—namely, that multiplicative noise ''works with the model'' to impact the model's variability. In other words, the model reacts to the components of the stochastic forcing that are optimal in terms of spatial or temporal distribution. In the DO model, if significant power is present with periods of 3–4 yr and if the phase of the stochastic forcing is optimal, the DO model responds with a large-amplitude ENSO. At all other times, the multiplicative noise damps the oscillations in the system. Despite the simplicity of the DO model compared to the GCM, we have demonstrated that a similar mechanism is at work in the CAM simulations; the SPPT scheme can simulate new WWB and trigger large El Niño events if the timing is right, but otherwise the enhanced stochasticity of westerly wind events results in a reduction of ENSO amplitude. Spatially, the multiplicative forcing systematically increases the amount of precipitation in regions with suppressed convection but has little impact in other regions.

Additive noise impacts the model more freely. The wavelet analysis carried out on the DO model indicates that for the additive noise case, a wide range of frequencies can affect the oscillations in the model and enhance the variability at a range of time scales. Such a free response to a stochastic forcing is not necessarily desirable, as it can result in modes of variability that are purely due to the nature of the forcing and not from the physics of the phenomenon as represented by the model's dynamical equations. For example, the low-frequency characteristics of the noise could introduce unphysical long-time-scale variations into the model. On the other hand, if the additive noise is carefully designed to represent a missing physical process, this could work to the modeler's advantage.

TABLE A1. Parameter setting used in the DO model for ENSO given in Eq. (A1).

Parameter	a	b	c	τ_1	τ_2	f_0	a_+	a_-	b_+	b_-	κ
Value	1/180	1/120	0.9/138	1.15 months	5.75 months	1/365 day^{-1}	1	1	1.5	0.3	1.4

The inclusion of a stochastic parameterization scheme improves the interannual variability of ENSO. We have shown that both additive and multiplicative stochastic forcing broaden the power spectrum of the DO model and that the multiplicative stochastic parameterization scheme (SPPT scheme) significantly improves the Niño-3.4 power spectrum in coupled runs of CAM4, by broadening the spectrum and reducing the overly periodic nature of ENSO. In general, it is known that the models in the CMIP5 ensemble show large systematic errors in the representation of ENSO, with serious deficiencies in ENSO variability; ''no major breakthrough'' was reported in the representation of ENSO in the CMIP5 ensemble compared to the CMIP3 ensemble (Flato et al. 2013). Many of the models produce an excessively periodic ENSO, with a Niño-3.4 power spectrum that is too sharp (Flato et al. 2013). It is an important next step to test the impact of SPPT in other coupled climate models to evaluate whether improving the interannual variability of ENSO is a systematic result or if it is specific to CAM. However, it is possible that the development and inclusion of stochastic parameterization schemes into coupled GCMs could be the very breakthrough needed to improve the representation of ENSO in the next generation of climate models.

Acknowledgments. The authors thank Paul Williams for helpful discussion and Stephan Juricke for his comments on a draft of the manuscript. We also thank two anonymous reviewers and Fei-Fei Jin for their constructive comments, which have significantly improved this manuscript. Several of the figures in this manuscript were made with help from the NCAR Climate Analysis Section's climate variability diagnostics package—the authors thank Adam Phillips for his support with using the package. Figure 4 was made using the MATLAB wavelet toolbox, written by A. Grinsted (available at http://www.glaciology.net/wavelet-coherence). The research of H.M.C. and T.N.P. was supported by European Research Council Grant 291406. The research of J.B. and D.R.B.C. was supported by the U.S. Environmental Protection Agency Grant G2011-STAR-D-183520501.

APPENDIX

Details of the Delayed Oscillator Model

a. Model details

The delayed oscillator (DO) model used in this study is taken from Stone et al. (1998) and is a simplification of the model presented in Münnich et al. (1991). The model describes the evolution of eastern Pacific thermocline depth anomaly $h(t)$ with time, where the anomaly is measured with respect to the seasonal average

$$\frac{dh}{dt} = aA[h(t-\tau_1)] - bA[h(t-\tau_2)] + c\cos(2\pi f_0 t) + cD_a\xi_a(t). \tag{A1}$$

The DO model has two delay terms. The first represents a Kelvin wave traveling to the eastern boundary with amplitude a, while the second term represents a Rossby wave traveling first to the western boundary, before being reflected as a Kelvin wave of amplitude b that travels to the eastern boundary. The delay times represent the velocities of these different waves and are set such that $\tau_1 = 1.15$ months and $\tau_2 = 5\tau_1$. The third term represents the effect of the annual cycle, with forcing amplitude c and frequency $f_0 = 1/12$ month^{-1}, while the fourth term represents an additive stochastic forcing: ξ_a is Gaussian, zero-mean, white noise, and D_a sets the amplitude of this additive forcing with respect to the seasonal cycle. The function $A(h)$ describes the forcing on the thermocline depth due to wind stress:

$$A(h) = \begin{cases} b_+ + \dfrac{b_+}{a_+}\left\{\tanh\left[\dfrac{\kappa_s a_+}{b_+}(h-h_+)\right]-1\right\}, & h_+ < h \\ \kappa_s h, & h_- \le h \le h_+ \\ -b_- - \dfrac{b_-}{a_-}\left\{\tanh\left[\dfrac{\kappa_s a_-}{b_-}(h_- - h)\right]-1\right\}, & h < h_- \end{cases} \tag{A2}$$

where $a_{\pm} \geq 1$ and continuity of $A(h)$ is ensured by setting

$$h_+ = \frac{b_+}{\kappa a_+}(a_+ - 1) \quad \text{and} \quad h_- = \frac{-b_-}{\kappa a_-}(a_- - 1). \tag{A3}$$

The κ parameter determines the strength of the ocean–atmosphere coupling. The impact of multiplicative noise in the atmosphere—for example, increased variability in westerly wind with increasing mean wind speed—is represented by multiplying the coupling parameter by a stochastic forcing term to give κ_s:

$$\kappa_s = [1 + cD_m\xi_m(t)]\kappa, \tag{A4}$$

where ξ_m is Gaussian, zero-mean, white noise, and D_m sets the amplitude with respect to the seasonal cycle. After removing the first 500 years of the integration to remove transients due to the initial conditions, the DO model is integrated for 10 000 years using a fourth-order Runge–Kutta (RK4) time-stepping scheme with a time step of $dt = 0.5$ days. As in Stone et al. (1998), the time series is smoothed using a 12-month running average to remove seasonal variations. The smoothed solution for the zero-noise case, $D_a = D_m = 0$, is shown in Fig. 4a for the values of the parameters shown in Table A1; for this value of κ, the system undergoes regular quasi-periodic oscillations with a characteristic period of 3 yr. Note that for the chosen parameter values $h_+ = h_- = 0$.

b. Wavelet analysis

Wavelet analysis is used to understand the interaction between the applied additive or multiplicative noise and the DO model. The time series are first smoothed using a 12-month running average, before a CWT is applied to each time series using an analytic Morlet wavelet; the resultant CWT indicates the frequency characteristics of the signals as a function of time (Grinsted et al. 2004; Mallat 2008). This provides more information about the time series than a Fourier transform, as it indicates localized changes in the frequency characteristics of the signals. The statistical significance of the peaks in the decomposition is calculated by comparing the wavelet power in frequency–time space to that generated by an AR(1) process with the same lag-1 autocorrelation, following Grinsted et al. (2004).

The wavelet cross spectrum $C_{x,y}$ allows detection of common behavior between the two time series by finding regions in time–frequency space where both time series have high power. It is defined as follows:

$$C_{x,y}(a,b) = C_x^*(a,b)C_y(a,b), \tag{A5}$$

where $C_x(a, b)$ is the CWT of x at time and frequency scales a and b and the star denotes the complex conjugate (Grinsted et al. 2004). The wavelet coherence (COH) finds regions where the time series covary but do not necessarily have high power. It is defined as follows:

$$\text{COH} = \frac{S[C_{x,y}(a,b)]}{\sqrt{S[|C_x(a,b)|^2]}\sqrt{S[|C_y(a,b)|^2]}}, \tag{A6}$$

where S is a smoothing operator in time and frequency space (Grinsted et al. 2004). The amplitude of COH effectively measures the local correlation between the two signals in time–frequency space, while the phase of COH indicates the phase offset between the two time series (Grinsted et al. 2004). The statistical significance of the wavelet coherence is estimated using the Monte Carlo technique described in Grinsted et al. (2004).

REFERENCES

Barnett, T. P., and R. W. Preisendorfer, 1987: Origins and levels of monthly and seasonal forecast skill for North American surface temperature determined by canonical correlation analysis. *Mon. Wea. Rev.*, **115**, 1825–1850, doi:10.1175/1520-0493(1987)115<1825:OALOMA>2.0.CO;2.

Berner, J., F. J. Doblas-Reyes, T. N. Palmer, G. Shutts, and A. Weisheimer, 2008: Impact of a quasi-stochastic cellular automaton backscatter scheme on the systematic error and seasonal prediction skill of a global climate model. *Philos. Trans. Roy. Soc. London*, **366A**, 2561–2579, doi:10.1098/rsta.2008.0033.

——, G. J. Shutts, M. Leutbecher, and T. N. Palmer, 2009: A spectral stochastic kinetic energy backscatter scheme and its impact on flow-dependent predictability in the ECMWF ensemble prediction system. *J. Atmos. Sci.*, **66**, 603–626, doi:10.1175/2008JAS2677.1.

——, T. Jung, and T. N. Palmer, 2012: Systematic model error: The impact of increased horizontal resolution versus improved stochastic and deterministic parameterizations. *J. Climate*, **25**, 4946–4962, doi:10.1175/JCLI-D-11-00297.1.

——, K. R. Fossell, S.-Y. Ha, J. P. Hacker, and C. Snyder, 2015: Increasing the skill of probabilistic forecasts: Understanding performance improvements from model-error representations. *Mon. Wea. Rev.*, **143**, 1295–1320, doi:10.1175/MWR-D-14-00091.1.

——, and Coauthors, 2016: Stochastic parameterization: Toward a new view of weather and climate models. *Bull. Amer. Meteor. Soc.*, doi:10.1175/BAMS-D-15-00268.1, in press.

Bove, M. C., J. B. Elsner, C. W. Landsea, X. Niu, and J. J. O. Brien, 1998: Effect of El Niño on U.S. landfalling hurricanes, revisited. *Bull. Amer. Meteor. Soc.*, **79**, 2477–2482, doi:10.1175/1520-0477(1998)079<2477:EOENOO>2.0.CO;2.

Braconnot, P., F. Hourdin, S. Bony, J. Dufresne, J. Grandpeix, and O. Marti, 2007: Impact of different convective cloud schemes on the simulation of the tropical seasonal cycle in a coupled ocean–atmosphere model. *Climate Dyn.*, **29**, 501–520, doi:10.1007/s00382-007-0244-y.

Buizza, R., M. Miller, and T. N. Palmer, 1999: Stochastic representation of model uncertainties in the ECMWF ensemble prediction system. *Quart. J. Roy. Meteor. Soc.*, **125**, 2887–2908, doi:10.1002/qj.49712556006.

Chang, P., L. Ji, H. Li, and M. Flügel, 1996: Chaotic dynamics versus stochastic processes in El Niño-Southern Oscillation in coupled ocean-atmosphere models. *Physica D*, **98**, 301–320, doi:10.1016/0167-2789(96)00116-9.

Chen, D., and Coauthors, 2015: Strong influence of westerly wind bursts on El Niño diversity. *Nat. Geosci.*, **8**, 339–345, doi:10.1038/ngeo2399.

Chiang, J. C. H., S. E. Zebiak, and M. A. Cane, 2001: Relative roles of elevated heating and surface temperature gradients in driving anomalous surface winds over tropical oceans. *J. Atmos. Sci.*, **58**, 1371–1394, doi:10.1175/1520-0469(2001)058<1371:RROEHA>2.0.CO;2.

Christensen, H. M., I. M. Moroz, and T. N. Palmer, 2015: Simulating weather regimes: Impact of stochastic and perturbed parameter schemes in a simple atmospheric model. *Climate Dyn.*, **44**, 2195–2214, doi:10.1007/s00382-014-2239-9.

Compo, G. P., and Coauthors, 2011: The Twentieth Century Reanalysis Project. *Quart. J. Roy. Meteor. Soc.*, **137**, 1–28, doi:10.1002/qj.776.

Danabasoglu, G., S. C. Bates, B. P. Briegleb, S. R. Jayne, M. Jochum, W. G. Large, S. Peacock, and S. G. Yeager, 2012: The CCSM4 ocean component. *J. Climate*, **25**, 1361–1389, doi:10.1175/JCLI-D-11-00091.1.

Dawson, A., and T. N. Palmer, 2015: Simulating weather regimes: impact of model resolution and stochastic parametrisation. *Climate Dyn.*, **44**, 2177–2193, doi:10.1007/s00382-014-2238-x.

Dee, D. P., and Coauthors, 2011: The ERA-Interim reanalysis: Configuration and performance of the data assimilation system. *Quart. J. Roy. Meteor. Soc.*, **137**, 553–597, doi:10.1002/qj.828.

Eisenman, I., L. Yu, and E. Tziperman, 2005: Westerly wind bursts: ENSO's tail rather than the dog? *J. Climate*, **18**, 5224–5238, doi:10.1175/JCLI3588.1.

Flato, G., and Coauthors, 2013: Evaluation of climate models. *Climate Change 2013: The Physical Science Basis*, T. F. Stocker et al., Eds., Cambridge University Press, 741–866.

Flügel, M., P. Chang, and C. Penland, 2004: The role of stochastic forcing in modulating ENSO predictability. *J. Climate*, **17**, 3125–3140, doi:10.1175/1520-0442(2004)017<3125:TROSFI>2.0.CO;2.

Frankcombe, L. M., H. A. Dijkstra, and A. S. von der Heydt, 2010: The Atlantic multidecadal oscillation: A stochastic dynamical systems view. *Stochastic Physics and Climate Modelling*, T. N. Palmer and P. Williams, Eds., Cambridge University Press, 287–306.

Gent, P. R., and Coauthors, 2011: The Community Climate System Model version 4. *J. Climate*, **24**, 4973–4991, doi:10.1175/2011JCLI4083.1.

Grieger, B., and M. Latif, 1994: Reconstruction of the El Niño attractor with neural networks. *Climate Dyn.*, **10**, 267–276, doi:10.1007/BF00228027.

Grinsted, A., J. C. Moore, and S. Jevrejeva, 2004: Application of the cross wavelet transform and wavelet coherence to geophysical time series. *Nonlinear Processes Geophys.*, **11**, 561–566, doi:10.5194/npg-11-561-2004.

Guilyardi, E., A. Wittenberg, A. Fedorov, M. Collins, C. Wang, A. Capotondi, G. J. van Oldenborgh, and T. Stockdale, 2009: Understanding El Niño in ocean–atmosphere general circulation models: Progress and challenges. *Bull. Amer. Meteor. Soc.*, **90**, 325–340, doi:10.1175/2008BAMS2387.1.

Hasselmann, K., 1976: Stochastic climate models: Part I. Theory. *Tellus*, **28A**, 473–485, doi:10.1111/j.2153-3490.1976.tb00696.x.

Huffman, G. J., R. F. Adler, D. T. Bolvin, and G. Gu, 2009: Improving the global precipitation record: GPCP version 2.1. *Geophys. Res. Lett.*, **36**, L17808, doi:10.1029/2009GL040000.

Hunke, E. C., and W. H. Lipscomb, 2008: CICE: The Los Alamos Sea Ice Model user's manual, version 4. Los Alamos National Laboratory Tech. Rep. LA-CC-06-012, 76 pp.

Jin, F.-F., J. D. Neelin, and M. Ghil, 1996: El Nino/Southern Oscillation and the annual cycle: Subharmonic frequency locking and aperiodicity. *Physica D*, **98**, 442–465, doi:10.1016/0167-2789(96)00111-X.

——, L. Lin, A. Timmermann, and J. Zhao, 2007: Ensemble-mean dynamics of the ENSO recharge oscillator under state-dependent stochastic forcing. *Geophys. Res. Lett.*, **34**, L03807, doi:10.1029/2006GL027372.

Kay, J. E., and Coauthors, 2015: The Community Earth System Model (CESM) large ensemble project: A community resource for studying climate change in the presence of internal climate variability. *Bull. Amer. Meteor. Soc.*, **96**, 1333–1349, doi:10.1175/BAMS-D-13-00255.1.

Kleeman, R., and A. M. Moore, 1997: A theory for the limitation of ENSO predictability due to stochastic atmospheric transients. *J. Atmos. Sci.*, **54**, 753–767, doi:10.1175/1520-0469(1997)054<0753:ATFTLO>2.0.CO;2.

Lawrence, D. M., and Coauthors, 2011: Parameterization improvements and functional and structural advances in version 4 of the Community Land Model. *J. Adv. Model Earth Syst.*, **3**, 2011MS000045, doi:10.1029/2011MS00045.

Levine, A. F. Z., and F.-F. Jin, 2010: Noise-induced instability in the ENSO recharge oscillator. *J. Atmos. Sci.*, **67**, 529–542, doi:10.1175/2009JAS3213.1.

——, and ——, 2015: A simple approach to quantifying the noise–ENSO interaction. Part I: Deducing the state-dependency of the windstress forcing using monthly mean data. *Climate Dyn.*, doi:10.1007/s00382-015-2748-1, in press.

Lin, J. W.-B., and J. D. Neelin, 2000: Influence of a stochastic moist convective parametrization on tropical climate variability. *Geophys. Res. Lett.*, **27**, 3691–3694, doi:10.1029/2000GL011964.

——, and ——, 2003: Towards stochastic deep convective parameterization in general circulation models. *Geophys. Res. Lett.*, **30**, 1162, doi:10.1029/2002GL016203.

Mallat, S., 2008: *A Wavelet Tour of Signal Processing*. 3rd ed. Academic Press, 832 pp.

McWilliams, J., and P. Gent, 1978: A coupled air and sea model for the tropical Pacific. *J. Atmos. Sci.*, **35**, 962–989, doi:10.1175/1520-0469(1978)035<0962:ACAASM>2.0.CO;2.

Moore, A. M., and R. Kleeman, 1999: Stochastic forcing of ENSO by the intraseasonal oscillation. *J. Climate*, **12**, 1199–1220, doi:10.1175/1520-0442(1999)012<1199:SFOEBT>2.0.CO;2.

Münnich, M., M. A. Cane, and S. E. Zebiak, 1991: A study of self-excited oscillations of the tropical ocean–atmosphere system. Part II: Nonlinear case. *J. Atmos. Sci.*, **48**, 1238–1248, doi:10.1175/1520-0469(1991)048<1238:ASOSEO>2.0.CO;2.

Neale, R. B., J. H. Richter, and M. Jochum, 2008: The impact of convection on ENSO: From a delayed oscillator to a series of events. *J. Climate*, **21**, 5904–5924, doi:10.1175/2008JCLI2244.1.

Neelin, J. D., 1990: A hybrid coupled general circulation model for El Niño studies. *J. Atmos. Sci.*, **47**, 674–693, doi:10.1175/1520-0469(1990)047<0674:AHCGCM>2.0.CO;2.

——, D. S. Battisti, A. C. Hirst, F.-F. Jin, Y. Wakata, T. Yamagata, and S. E. Zebiak, 1998: ENSO theory. *J. Geophys. Res.*, **103**, 14 261–14 290, doi:10.1029/97JC03424.

Palmer, T. N., R. Buizza, F. Doblas-Reyes, T. Jung, M. Leutbecher, G. J. Shutts, M. Steinheimer, and A. Weisheimer, 2009: Stochastic parametrization and model uncertainty. ECMWF Tech. Rep.

598, 44 pp. [Available online at http://www.ecmwf.int/sites/default/files/elibrary/2009/11577-stochastic-parametrization-and-model-uncertainty.pdf.]

Penland, C., 1996: A stochastic model of Indopacific sea surface temperature anomalies. *Physica D*, **98**, 534–558, doi:10.1016/0167-2789(96)00124-8.

——, and P. D. Sardeshmukh, 1995: The optimal growth of tropical sea surface temperature anomalies. *J. Climate*, **8**, 1999–2024, doi:10.1175/1520-0442(1995)008<1999:TOGOTS>2.0.CO;2.

Phillips, A. S., C. Deser, and J. Fasullo, 2014: A new tool for evaluating modes of variability in climate models. *Eos, Trans. Amer. Geophys. Union*, **95**, 453–455, doi:10.1002/2014EO490002.

Rasmusson, E. M., and T. H. Carpenter, 1982: Variations in tropical sea surface temperature and surface wind fields associated with the Southern Oscillation/El Niño. *Mon. Wea. Rev.*, **110**, 354–384, doi:10.1175/1520-0493(1982)110<0354:VITSST>2.0.CO;2.

Rayner, N. A., D. E. Parker, E. B. Horton, C. K. Folland, L. V. Alexander, D. P. Rowell, E. C. Kent, and A. Kaplan, 2003: Global analyses of sea surface temperature, sea ice, and night marine air temperature since the late nineteenth century. *J. Geophys. Res.*, **108**, 4407, doi:10.1029/2002JD002670.

Ropelewski, C. F., and M. S. Halpert, 1987: Global and regional scale precipitation patterns associated with the El Niño/Southern Oscillation. *Mon. Wea. Rev.*, **115**, 1606–1626, doi:10.1175/1520-0493(1987)115<1606:GARSPP>2.0.CO;2.

——, and ——, 1996: Quantifying Southern Oscillation–precipitation relationships. *J. Climate*, **9**, 1043–1059, doi:10.1175/1520-0442(1996)009<1043:QSOPR>2.0.CO;2.

Roulston, M. S., and J. D. Neelin, 2000: The response of an ENSO model to climate noise, weather noise and intraseasonal forcing. *Geophys. Res. Lett.*, **27**, 3723–3726, doi:10.1029/2000GL011941.

Sarachik, E. S., and M. A. Cane, 2010: *The El Niño–Southern Oscillation Phenomenon.* Cambridge University Press, 384 pp.

Sardeshmukh, P. D., 2005: Issues in stochastic parameterization. *Proc. Workshop on Representation of Sub-Grid Processes Using Stochastic-Dynamic Models*, Shinfield Park, Reading, ECMWF, 5–12.

——, C. Penland, and M. Newman, 2001: Rossby waves in a stochastically fluctuating medium. *Stochastic Climate Models*, P. Imkeller and J.-S. von Storch, Eds., Birkhaueser, 359–384.

——, ——, and ——, 2003: Drifts induced by multiplicative red noise with application to climate. *Europhys. Lett.*, **63**, 498–504, doi:10.1209/epl/i2003-00550-y.

Shutts, G., 2005: A kinetic energy backscatter algorithm for use in ensemble prediction systems. *Quart. J. Roy. Meteor. Soc.*, **131**, 3079–3102, doi:10.1256/qj.04.106.

Stone, L., P. I. Saparin, H. Huppert, and C. Price, 1998: El Niño chaos: The role of noise and stochastic resonance on the ENSO cycle. *Geophys. Res. Lett.*, **25**, 175–178, doi:10.1029/97GL53639.

Suarez, M. J., and P. S. Schopf, 1988: A delayed action oscillator for ENSO. *J. Atmos. Sci.*, **45**, 3283–3287, doi:10.1175/1520-0469(1988)045<3283:ADAOFE>2.0.CO;2.

Sun, D.-Z., Y. Yu, and T. Zhang, 2009: Tropical water vapor and cloud feedbacks in climate models: A further assessment using coupled simulations. *J. Climate*, **22**, 1287–1304, doi:10.1175/2008JCLI2267.1.

Tompkins, A. M., and J. Berner, 2008: A stochastic convective approach to account for model uncertainty due to unresolved humidity variability. *J. Geophys. Res.*, **113**, D18101, doi:10.1029/2007JD009284.

Tziperman, E., and L. Yu, 2007: Quantifying the dependence of westerly wind bursts on the large-scale tropical Pacific SST. *J. Climate*, **20**, 2760–2768, doi:10.1175/JCLI4138a.1.

Vose, R. S., and Coauthors, 2012: NOAA's merged land–ocean surface temperature analysis. *Bull. Amer. Meteor. Soc.*, **93**, 1677–1685, doi:10.1175/BAMS-D-11-00241.1.

Weisheimer, A., S. Corti, T. N. Palmer, and F. Vitart, 2014: Addressing model error through atmospheric stochastic physical parametrizations: Impact on the coupled ECMWF seasonal forecasting system. *Philos. Trans. Roy. Soc. London*, **372A**, 20130290, doi:10.1098/rsta.2013.0290.

Williams, P. D., 2012: Climatic impacts of stochastic fluctuations in air–sea fluxes. *Geophys. Res. Lett.*, **39**, L10705, doi:10.1029/2012GL051813.

Wu, Z., E. S. Sarachik, and D. S. Battisti, 1999: Thermally forced surface winds on an equatorial beta plane. *J. Atmos. Sci.*, **56**, 2029–2037, doi:10.1175/1520-0469(1999)056<2029:TFSWOA>2.0.CO;2.

Yeh, S.-W., and B. Kirtman, 2006: Origin of decadal El Niño–Southern Oscillation–like variability in a coupled general circulation model. *J. Geophys. Res.*, **111**, C01009, doi:10.1029/2005JC002985.

Zebiak, S. E., and M. A. Cane, 1987: A model El Niño–Southern Oscillation. *Mon. Wea. Rev.*, **115**, 2262–2278, doi:10.1175/1520-0493(1987)115<2262:AMENO>2.0.CO;2.